DYNAMIC RESPONSE OF LATERALLY LOADED OFFSHORE PILING

Prepared by

HAYES E. ROSS, JR.

Structural Research Division

Texas Engineering Experiment Station

TAMU-SG-70-224 August 1970 COE REPORT No. 132

DYNAMIC RESPONSE OF LATERALLY LOADED OFFSHORE PILING

by

Hayes E. Ross, Jr.
Structural Research Division
Civil Engineering Department
Texas A&M University

Partially Supported by the National Science Foundation
Sea Grant Program
Institutional Grant GH-26 to
Texas A&M University

Sea Grant Publication No. TAMU-SG-70-224
Coastal and Ocean Engineering Division
Report No. 132 - C.O.E.

August 1970

PREFACE

In September, 1968, an analytical study of the dynamic response of laterally loaded offshore piles was begun. The one year project was partially funded by the National Science Foundation Sea Grant Program institutional grant GH-26 made to Texas A&M University. This report describes the developments of that study. In addition, the writer used the contents of this paper to fulfill the dissertation requirements of his Doctor of Philosophy degree at Texas A&M University.

As a continuing study, Texas A&M University received support from the National Science Foundation Sea Grant Program for 1969 through 1970 through institutional grant GH-59 to investigate the static and dynamic resistance of a cohesive soil when loaded laterally by a pile. The results, now receiving final evaluation, will provide valuable input to the mathematical model described herein. A similar study on cohesiveless soils was begun in September, 1970. This one year study will also be partially funded by the National Science Foundation Sea Grant Program through institutional grant GH-101.

ABSTRACT

A mathematical model which describes the dynamic response of a laterally loaded offshore pile was developed in this research. Interaction effects between the pile and its water environment were considered in formulating the problem. Also considered were the nonlinear material properties of the soil and the geometrical nonlinearity of the pile. A discrete element system was utilized in idealizing the pile, soil, and water medium. Airy wave theory was used to describe the wave kinematics and Morison's equation was used to describe wave kinetics.

To solve the second-order nonlinear differential equations of motion of the system, the fourth-order Runge-Kutta numerical integration method was applied. Matrix notation was used in formulating the problem and a computer program was written to provide numerical solutions.

Dynamic tests were conducted on three different size model piles and the results were compared with simulated results from the mathematical model. A close comparison verified the accuracy of the model and analysis employed.

Parameter studies were conducted to determine the influence of some of the significant factors on the pile's response. The effects of soil modulus of subgrade reaction, soil damping, wave-pile interaction, and axial load in the pile were investigated. A typical offshore pile was utilized in the studies.

TABLE OF CONTENTS

		Page
	PREFACE	ii
	ABSTRACT	iii
	TABLE OF CONTENTS	iv
	LIST OF FIGURES	vi
	LIST OF TABLES	viii
I.	INTRODUCTION	1
	1.1 General	1
	1.2 Literature Review	3
	Pile medium	3
	Water wave medium	3
	Soil medium	4
	Interaction between the three media	6
	1.3 Procedure	10
II.	THE IDEALIZED MODEL	12
	2.1 General	12
	2.2 Pile Medium	13
	2.3 Water Wave Medium	22
	2.4 Soil Medium	29
	2.5 Equations of Motion	36
III.	NUMERICAL SOLUTION TECHNIQUES	40
	3.1 General	40
	Recursion method	40
	Milne predictor-corrector method	40
	Runge-Kutta method	41
	3.2 Summary	42
IV.	VALIDATION STUDY	44
	4.1 General	44
	4.2 Analytical Study	44
	4.3 Structural Damping Study	46
	4.4 Model Pile Studies	47
	Static tests	47
	Dynamic tests	51

TABLE OF CONTENTS (CONTINUED)

		Page
	4.5 Comparison of Field Tests with Model Predictions	52
V.	PARAMETER STUDIES	65
	5.1 General	65
	5.2 Distribution of Modulus of Subgrade Reaction	65
	5.3 Soil Damping	70
	5.4 Static versus Dynamic Displacements	70
	5.5 Wave-Structure Interaction	72
	5.6 Axial Load Effects	76
VI.	CONCLUSIONS	79
VII.	RECOMMENDATIONS	81
	REFERENCES	83
	APPENDIX I COMPUTER PROGRAM DESCRIPTION	88
	APPENDIX II COMPUTER PROGRAM INPUT	93
	APPENDIX III NOTATION	107

LIST OF FIGURES

		Page
2.1	PILE IDEALIZATION	14
2.2	PILE SEGMENT	16
2.3	NODE i DEGREES OF FREEDOM	20
2.4	EQUIVALENT PLATFORM STIFFNESS	21
2.5	WAVE DEFINITION SKETCH (AIRY THEORY)	27
2.6	SOIL RHEOLOGICAL MODEL AT NODE m	30
2.7	SYSTEM IDEALIZATION	37
4.1	ELASTIC MODEL	45
4.2	RELATION BETWEEN STRUCTURAL DAMPING AND CRITICAL DAMPING	48
4.3	PIPE CONFIGURATION	49
4.4	LOAD DEFORMATION RESULTS, 2.0 INCH PIPE	50
4.5	GENERAL PIPE IDEALIZATION	53
4.6	DISPLACEMENT VERSUS SOIL MODULUS, 2.0 INCH PIPE	55
4.7	FUNDAMENTAL FREQUENCY VERSUS SOIL MODULUS, 2.0 INCH PIPE	57
4.8	ACCELERATION VERSUS TIME, 3.0 INCH PIPE	60
4.9	ACCELERATION VERSUS TIME, 2.0 INCH PIPE	61
4.10	ACCELERATION VERSUS TIME, 1.5 INCH PIPE	62
5.1	TYPICAL PILE AND ITS IDEALIZATION	66
5.2	SUBGRADE MODULUS DISTRIBUTION	68
5.3	NODE 6 DISPLACEMENT VERSUS TIME, SUBGRADE MODULUS STUDY	69

LIST OF FIGURES (CONTINUED)

		Page
5.4	NODE 9 DISPLACEMENT VERSUS TIME, SOIL DAMPING STUDY	71
5.5	MAXIMUM DISPLACEMENTS, CASE B	73
5.6	NODE 1 DISPLACEMENT VERSUS TIME, INTERACTION STUDY	74
5.7	NODE 6 DISPLACEMENT VERSUS TIME, INTERACTION STUDY	75
5.8	NODE 6 DISPLACEMENT VERSUS TIME, AXIAL LOAD STUDY	77
A1	FLOW CHART	90

LIST OF TABLES

		Page
4.1	ELASTIC MODEL COMPARISONS	45
4.2	PIPE DIMENSIONS AND PROPERTIES	49
4.3	STATIC LOAD DATA	51
4.4	IDEALIZED PIPE DATA	54
5.1	SUBGRADE DISTRIBUTION DATA	68
A1	RUNGE-KUTTA CASE CHARACTERISTICS	92

CHAPTER I

INTRODUCTION

1.1 General

Offshore exploration for crude petroleum has increased at a steady pace for the last ten years. Drilling platforms have been located in deeper and deeper water to keep pace with the ever-increasing demand for oil and its by-products. Defense installations and weather recording devices have been placed offshore for obvious reasons. This expanding offshore activity has met with an increase in design complexities since hydrostatic and hydrodynamic forces increase in the deeper water.

Many offshore structures are supported by piles driven into the bed of the ocean. Frequently, the critical factor in the design of these structures is the lateral dynamic loading from waves. In the past, little consideration has been given to the dynamic effects of wave forces on structural integrity. This lack of consideration was not an oversight on the part of design engineers but rather was due largely to the complexity of the problem and the lack of high-speed computers needed to solve such problems.

Knowledge of the interaction between the pile and its water and soil environment is a requisite to accurately compute the response of a pile-supported offshore structure. This research

The citations on the following pages follow the style of the Journal of the Structural Division, Proceedings of the American Society of Civil Engineers.

attempts to fill this need by developing an analytical method of predicting the dynamic response of offshore piling.

Although this research is primarily concerned with offshore piling, it has applications in other areas. For example, the marine riser on an offshore drilling platform is subjected to wave action between the platform and the bed of the sea. A floating rig which extracts samples or drills for oil may operate in water of considerable depth and its riser may experience high dynamic loads.

It was apparent after a review of the literature that published reports on the dynamic response of piling due to wave action, taking into account the interaction effects between the pile and its water and soil environment, were practically nonexistent. The need for such an investigation became quite evident.

To date, considerable effort has been expended in the field of soil-structure interaction, particularly under static loads and in some cases under dynamic loads. In laterally loaded pile studies the usual approach to the problem has been through experimental analysis, by either prototype or model. Economically, experimental analysis is often undesirable. Another undesirable feature is that the results are usually applicable to only the type of piles tested.

In most analytical studies found in the literature, inherent assumptions usually limit their results to special cases in which the soil and pile behave as linear elastic systems. For some applications, these assumptions may lead to relatively accurate

results, while in others they may result in completely erroneous conclusions. At present the uncertainty remains, especially in dynamic analysis.

1.2 Literature Review

After studying much of the literature in the field of structural dynamics, it was learned there was no precedent for the particular problem undertaken in this investigation. That is not to say that the work of others in related studies could not be exploited. Since this research embraces the work of three distinct disciplines, namely structural mechanics, hydromechanics, and soil mechanics, the writer felt it appropriate to review the basic literature in each field as related to this research and review the work concerning their interaction.

Pile medium. Recent advances in high-speed computers have resulted in a general acceptance of the "finite element" method of analysis for structural problems heretofore regarded as unsolvable. Numerous publications (18,33,43) are available to aid in applying this method to the problem at hand, i.e., the structural idealization of the pile medium for dynamic analysis.

Water wave medium. Since the studies of Morison, et al, (29) it is common practice to compute wave forces on piles by separating the total resistance force into two components, a drag force and an inertia or mass force. Needed in computing these force components are drag and inertia coefficients corresponding to a particular

wave theory and pile size. The major problem lies in selecting one of a number of available theories and subsequently calculating the required information, which, for higher order theories, is a relatively complicated procedure.

The work of Dean (4,5) presents criteria which can be used to assess the validity of various wave theories and attempts to establish the particular theories providing best boundary condition fits for wave conditions of engineering significance. The interested reader may also refer to the former paper for a good bibliography on the different wave theories. Dean's work is a significant step forward in reducing the uncertainties involved in the computation of wave forces on offshore structures.

After selecting the appropriate wave theory, drag and inertia coefficients are established. Several sources (1,42,6) may be referred to for this purpose. The latter reference offers the most recent comparison of available coefficients, and it also contains a good reference list documenting many of the studies conducted in this field.

Soil medium. Analytic description of soil behavior continues to be a challenge to the scientist and engineer. The generally accepted approach is to conveniently define a rheological model which will simulate to a reasonable degree the behavior of the soil under analysis. The task of determining such a model is generally far from simple and to date no widely accepted model has been devised.

To define the resistance of a material to dynamic loading, Lord Kelvin originally expressed it in terms of a static plus a dynamic component. Voight derived the mathematical relation for the rheological model of Kelvin, from which the well known Kelvin-Voight model originated. As a seemingly logical choice, many engineers have utilized the Kelvin-Voight model in soil mechanics for some time.

In recent years, Smith (38) and Samson, Hirsch, and Lowery (23, 36) have successfully used a form of the Kelvin-Voight model in pile driving analysis. One of the uncertainties these researchers met in applying this model was the amount by which the soil damped out the pile's motion. Gibson and Coyle (11) have attempted to shed some light on this problem.

Penzien, et al, (31) used a form of the Kelvin-Voight model in studying the response of a pile-supported bridge to seismic disturbances. Their work was of particular interest since it included a determination of the dynamic response of laterally loaded piles. Other researchers (15,19,21,40) in the field of earthquake engineering have made significant contributions which will aid in understanding the dynamic properties of soil.

Chan and Hirsch (3) published an annotated bibliography concerning available data on soil dynamics and soil rheology. It is a concise and convenient source of information on the subject, covering many important publications up to 1966.

Interaction between the three media. In the classic or exact approach, Timoshenko (41) has solved the problem of a vibrating elastic beam on a massless elastic foundation. As related to this investigation, Timoshenko's solution is mainly of academic nature but could possibly be used as a check on the accuracy of the numerical solution. Others have applied various boundary conditions to Timoshenko's solution but none have considered the effects of inelastic and nonlinear behavior of beam and foundation.

Matlock and Reese (25) developed a generalized solution for laterally loaded piles with static loads. The force-deformation characteristics of the soil were considered to be nonlinear and the solution to the differential equations was accomplished by an iterative procedure using repeated applications of elastic theory with the soil modulus constants being adjusted at each successive trial. Feibusch and Keith (7) utilized the solution of Matlock and Reese in deriving a method of analysis for statically loaded pile-supported offshore structures. Their analysis included the combined effects of the elastic structure and piles with the inelastic properties of the supporting soil.

The dynamic response of docking structures was investigated analytically by Michalos (27). A simplified approach to the problem was taken in that only a single degree-of-freedom system was considered with the point-of-fixity method being used to simulate the soil's lateral restraint. Subsequent discussions (34) of this paper questioned the value of such a simplified analysis

suggesting that a more accurate representation could be realized by accounting for the inelastic properties of the soil.

Spillers and Stoll (39) considered the effects of a continuous soil medium on the interaction of laterally loaded pile. Two idealized models were analyzed, (1) an elastic pile in an elastic half space, and (2) an elastic pile in an elasto-plastic half space. Use was made of the "Mindlin equation" (28) in determining soil properties relating deformations within the soil at specific points to the resulting soil forces. Their study was also limited to static load analysis.

The dynamic response to seismic disturbances of structures supported on long piles extending through deep sensitive clays was considered by Penzien, et al (31). Their method of analysis accounted for the interaction between the superstructure (a specific bridge structure) and its pile foundations and the interaction effects between the pile foundation and their surrounding clay media. Extensive soil tests were conducted and their results used to determine the nonlinear hysteretic stress-strain relations, damping characteristics, and the creep characteristics of the clay. In the study, an attempt was made to use the continuous soil medium approach of Spillers and Stoll (39) but after considerable effort had been spent the decision was made to simplify the problem by using uncoupled soil properties, often called the Winkler assumption. This approach led to an extremely complicated method of analysis which would have required a great effort to reach a solution.

In another study involving earthquake motions, Fleming, Screwvala, and Konder (8) conducted an analytical study which was concerned with the structure-soil interaction. The structure was idealized by a lumped mass mathematical model which is attached to the moving rock layer by a flexible member having the same force-displacement relationship as the foundation. The soil properties were assumed to be linearly elastic and the effect of soil damping was not considered. They conclude that in earthquake analysis completely erroneous results may occur if the foundation superstructure interaction is not considered.

One of the earliest studies in the dynamics of laterally loaded offshore piles was reported by Gaul (10). A dimensionally scaled model of a vertical pile in a weak marine foundation was dynamically tested by application of a time varying sinusoidal load, similar to that produced by ocean waves. Test results indicated that for "relatively" low frequencies of load oscillation no dynamic load factor is required to produce the same maximum subsurface bending moments in the pile under static and dynamic loading. As Gaul points out, however, the determination of reliable load factors by model studies would require testing over a wide range of forcing frequencies, types of piles, and types of foundations. Several other investigators (16,17,26,32) have conducted experimental studies of both model and prototype piles under dynamic loading.

Interest in the dynamic behavior of offshore structures increased considerably following the collapse of the Texas Tower

Number 4 radar platform in 1961, offshore from New Jersey. Its failure has been attributed to a resonance condition, initiated by waves whose heights were considerably less than what was considered to be the "design" wave height. In their study, Harleman, Nolan, and Honsinger (14) performed a dynamic analysis of an offshore structure in oscillatory waves, a structure similar to the Texas Tower. The structure was idealized as a single degree-of-freedom equivalent spring-mass system, with no soil-structure interaction considered. It was concluded that the highest wave to be expected in a given locality is not necessarily the critical design wave, giving credence to the postulated cause of failure in the Texas Tower.

Billington, Gaither, and Ebner (2) investigated the response of a three-dimensional four-legged tower subjected to wave loading by use of a mathematical model and an experimental model. The mathematical model consisted of lumped masses interconnected by weightless elastic springs. Distributed water damping forces were assumed to be linearly dependent upon velocity and internal damping was assumed to vary linearly with the frequency of the forcing function. Soil structure interaction was not considered. It is this author's opinion that these limitations greatly restrict the application of their results.

Three papers of interest were presented at a specialty conference in 1967, all three dealing with the dynamic response of offshore structures. In the first (9) of these papers an attempt was

made to study the system which produces waves, the kinetic and kinematic properties of the waves, the structural system, and its interaction with the water environment. The second paper (30) was concerned with the design of offshore bottom supported structures which are subject to both periodic and random wave forces. Both analytic and experimental studies were made. Among other results, an expression is presented from which the optimum support spacing for a structure built on four supports and an "adequate foundation" can be determined, resulting in minimum platform response. It was also concluded that for large diameter cylinders in deep water, the drag component in the Morison equation can be neglected. In the third paper (37) it was concluded that the three-dimensional behavior of an offshore structure is of importance and the interaction of structure and wave can be of consequence under certain circumstances. The importance of wave-structure interaction was also emphasized by Gomez-Rivas in a recent publication (13). It should be pointed out that none of these studies considered the effects of soil-structure interaction.

1.3 Procedure

Since there was a marked absence of information on the dynamic behavior of laterally loaded offshore piling the primary reason for conducting this study was to advance the "state-of-the-art." In so doing, the following procedure was followed:

1. An analytical solution was developed for the dynamic response of an offshore pile when subjected to wave forces, considering the interaction effects between the pile and its water and soil environment. Nonlinear properties of the soil and pile were considered. The solution was attained by applying numerical techniques to the differential equations of motion. A discrete parameter system was used to approximate the three continuous mediums, i.e., the pile, soil, and water.
2. Dynamic tests were performed on model piles and the results were compared to simulated results from the analytical solution.
3. The influence of significant parameters on the dynamic response was investigated.
4. The mathematical solution was applied to obtain the dynamic response of a typical offshore pile.

CHAPTER II

THE IDEALIZED MODEL

2.1 General

Although closed-form solutions exist for a class of vibrating elastic beams on massless elastic foundations constrained to particular boundary conditions, none exists for a pile (or beam) supported by a viscoelastic or viscoplastic media subjected to time-dependent excitation loads of the type found in water waves. The mathematical complexities of such an approach prohibit its consideration.

In lieu of an exact solution, the next logical step is to formulate an idealized or mathematical model based on approximations and simplified assumptions which will represent, within acceptable tolerances, the physical system. After a satisfactory model has been defined, the laws of mechanics dictate the mathematical formulation (the differential equations of motion in this case); and with the aid of matrix methods, numerical integration techniques, and a high-speed digital computer, a solution is usually possible. Laboratory and field test results are then relied on to determine its validity.

The following sections describe the idealizations chosen to represent the physical system of this problem, viz., the pile, water, and soil.

2.2 Pile Medium

The usual procedure for idealizing a continuum with an infinite number of degrees of freedom such as a pile with a distributed mass is to discretize or lump the continuum into a finite number of masses. This procedure is employed in this investigation. The lumped masses are interconnected by weightless elastic springs whose stiffnesses are determined by the force-deformation characteristics of the segmented pile elements.

The first step in the idealization is to segment the pile into a finite number of elements as shown in Figure 2.1. The juncture of two pile elements is termed a node, at which the distributed mass is lumped. Several factors must be considered when selecting the number of pile elements.

1. The chosen number of elements must represent a compromise between an exact representation of the real structure, which theoretically requires an infinite number, and the computer time required to reach a solution, which increases with increasing lumped masses.
2. Due to the nature of wave forces, described in a subsequent section, care must be taken in selecting the number and location of nodes along the length of pile between the wave's crest and trough and along the length immediately below the trough.

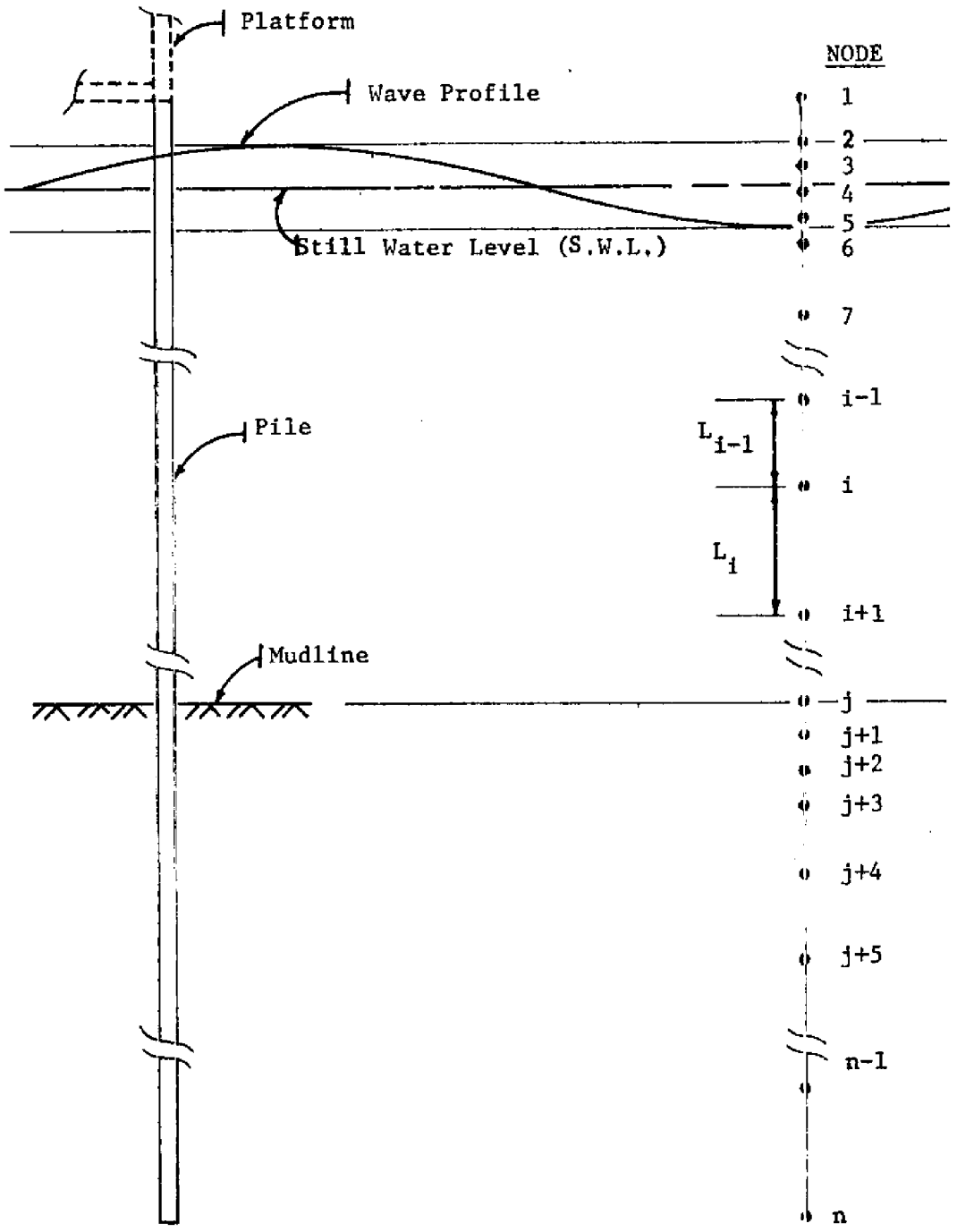

FIGURE 2.1 - PILE IDEALIZATION

3. The manner in which the soil resistance varies with depth may have an influence on the number and location of nodes below the mudline. As described subsequently, the soil's dynamic resistance is assumed to be localized at the respective nodes.
4. Many offshore piles have varying degrees of stiffness along their length. Most piles are stiffer in the vicinity of the mudline where the internal pile stresses are usually a maximum; this factor should be considered in the idealization.

After selecting the number and location of the nodes, the mass and stiffness matrix can be assembled. A simple procedure is used to lump the masses; half the mass of each segment is placed at the ends of the segments. Referring to Figure 2.1, the mass of node i is designated M_i, and is computed by Equation 2.1:

$$M_i = \frac{0.5(L_{i-1}w_{i-1} + L_i w_i)}{g} \qquad (2.1)$$

where, w_i = weight of segment i per unit length

g = gravitational acceleration

Note that the pile segment number is taken as the number of the node immediately above it. The total pile mass matrix, [M], a diagonal matrix, is the assemblage of all the lumped masses, i.e.,

$$[M] = \begin{bmatrix} M_1 & & & \\ & M_2 & & \\ & & \ddots & \\ & & & M_{n-1} \\ & & & & M_n \end{bmatrix} \qquad (2.2)$$

To account for the platform's inertia an equivalent platform mass was added to the lumped mass at node 1. Although this value may be difficult to determine, some provision must be made for its influence in establishing a reliable model of the pile-water-soil system. After this model is validated the next logical step would be a dynamic analysis of the entire structure, which would eliminate the need of defining an equivalent mass.

Force-deformation properties of the pile can be readily obtained by use of matrix methods. Consider the pile segment shown in Figure 2.2, which has a modulus of elasticity E, moment of inertia I, and cross-sectional area A, along its length.

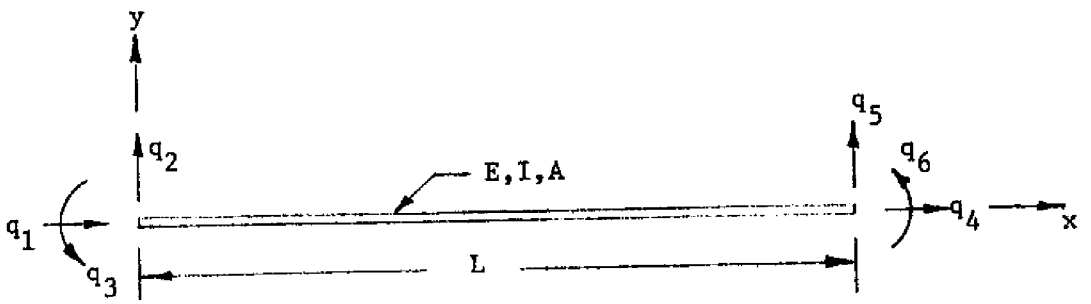

FIGURE 2.2 - PILE SEGMENT

The q's denote displacements of the segment ends in the x-y coordinate system, e.g., q_4 equals the displacement of the right end in the x direction. Only displacements in the x-y plane are considered. Stress resultants at the member ends are denoted by s subscripted in the same manner as q. If the material mechanical properties of the segment are linearly elastic, displacements are "small", and the axial load "small", then the stress resultants are linearly related to the displacements. The constants of proportionality relating stress to displacements are called the elastic member or segment stiffness matrix, denoted as $[k_e]$.

Most offshore structures are designed according to specifications which limit working stresses to a value below the material's elastic limit thus preventing material nonlinearity. Further, the specifications usually limit displacements to within what can be termed small displacements so that the equilibrium equations formulated for the undeformed configuration need not be modified for the deformed configuration. This analysis assumes that these two conditions, i.e., linearly elastic material properties and small displacements, are met.

It is generally known that the lateral stiffness of a structural member is dependent on its axial load. To account for the effects of axial load on the element's stiffness, use is made of the so-called element "geometrical matrix", $[k_g]$. A detailed description of its derivation can be found in the literature (33) and will not be given here.

The equations of equilibrium for the beam element can now be written as

$$\{s\} = [k_e]\{q\} + [k_g]\{q\} \tag{2.3}$$

where

$$[k_e] = \begin{bmatrix} \frac{AE}{L} & & & & & \\ 0 & \frac{12EI}{L^3} & & \text{SYMMETRICAL} & & \\ 0 & \frac{6EI}{L^2} & \frac{4EI}{L} & & & \\ -\frac{AE}{L} & 0 & 0 & \frac{AE}{L} & & \\ 0 & -\frac{12EI}{L^3} & -\frac{6EI}{L^2} & 0 & \frac{12EI}{L^3} & \\ 0 & \frac{6EI}{L^2} & \frac{2EI}{L} & 0 & -\frac{6EI}{L^2} & \frac{4EI}{L} \end{bmatrix} \tag{2.4}$$

and

$$[k_g] = \frac{F}{L}\begin{bmatrix} 0 & & & & & \\ 0 & \frac{6}{5} & & & & \\ 0 & \frac{L}{10} & \frac{2L^2}{15} & & \text{SYMMETRICAL} & \\ 0 & 0 & 0 & 0 & & \\ 0 & -\frac{6}{5} & -\frac{L}{10} & 0 & \frac{6}{5} & \\ 0 & \frac{L}{10} & -\frac{L^2}{30} & 0 & -\frac{L}{10} & \frac{2L^2}{15} \end{bmatrix} \tag{2.5}$$

where

$$F = \frac{EA}{L}(q_4 - q_1) \tag{2.6}$$

Equation 2.3 can be rewritten as

$$\{s\} = [k_e + k_g]\{q\} \tag{2.7}$$

If the axial load, F, remains constant as lateral loads are applied, the element's stiffness, defined by $[k_e + k_g]$, remains constant. In this manner, $[k_g]$ acts to increase the lateral stiffness if the axial load creates tension in the element and reduces it if the axial load creates compression.

It is assumed that the axial load in each pile segment remains constant during a given event or analysis, although the axial load along the pile's length is permitted to change from segment to

and

$$[k_g] = \frac{F}{L}\begin{bmatrix} 0 & & & & & \\ 0 & \frac{6}{5} & & & & \\ 0 & \frac{L}{10} & \frac{2L^2}{15} & & \text{SYMMETRICAL} & \\ 0 & 0 & 0 & 0 & & \\ 0 & -\frac{6}{5} & -\frac{L}{10} & 0 & \frac{6}{5} & \\ 0 & \frac{L}{10} & -\frac{L^2}{30} & 0 & -\frac{L}{10} & \frac{2L^2}{15} \end{bmatrix} \tag{2.5}$$

where

$$F = \frac{EA}{L}(q_4 - q_1) \tag{2.6}$$

Equation 2.3 can be rewritten as

$$\{s\} = [k_e + k_g]\{q\} \tag{2.7}$$

If the axial load, F, remains constant as lateral loads are applied, the element's stiffness, defined by $[k_e + k_g]$, remains constant. In this manner, $[k_g]$ acts to increase the lateral stiffness if the axial load creates tension in the element and reduces it if the axial load creates compression.

It is assumed that the axial load in each pile segment remains constant during a given event or analysis, although the axial load along the pile's length is permitted to change from segment to

segment. Thus, for a known axial load and the mechanical and geometrical properties of the pile segments, each individual element stiffness matrix can be computed, herein denoted as [k].

$$[k] = [k_e + k_g] \tag{2.8}$$

After determining the stiffness matrix of each element, the stiffness matrix of the entire pile is assembled. Since the literature contains information on the procedure for this assemblage (33, 43), a detailed description is unnecessary.

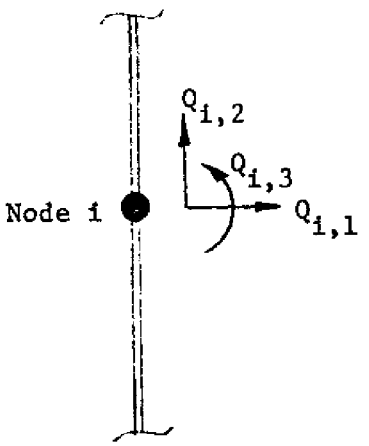

FIGURE 2.3 - NODE i DEGREES OF FREEDOM

Referring to Figure 2.3, Q_{ij} is used to denote a displacement at node i in the j direction. Similarly, S_{ij} is used to denote an external load at node i in the j direction. Equilibrium equations for the pile can therefore be written as

$$\{S\} = [K^P]\{Q\} \qquad (2.9)$$

where $[K^P]$ is the assembled stiffness matrix for the pile.

As mentioned previously, some consideration must be given to the influence that the platform has on the dynamic properties of the pile. Consider Figure 2.4.

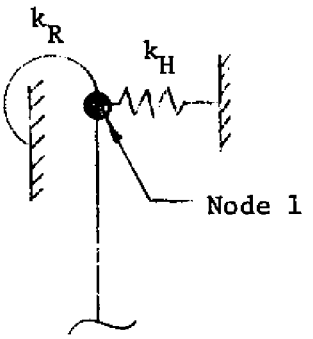

FIGURE 2.4 - EQUIVALENT PLATFORM STIFFNESS

As shown, k_H is used to denote the lateral stiffness offered by the platform and k_R its rotational restraint. Again, these values may be difficult to determine but their effect on the pile's response must be considered in an analysis of this type. The values of k_H and k_R are added to the appropriate elements of the stiffness matrix $[K^P]$.

Internal friction within the material of the pile results in structural damping. In an elastic system it is generally agreed that the structural damping force is directly proportional in

magnitude to the internal elastic force and acts in the opposite direction to the velocity vector. If the proportionality constant, μ, relating the damping forces $\{S_D\}$ to the elastic forces $\{S\}$ is assumed to be constant for all segments of the pile:

$$\{S_D\} = -\mu \left[\frac{\dot{Q}}{|\dot{Q}|}\right] \{|S|\} \tag{2.10}$$

where the dot represents a derivative with respect to time. Substituting the value of $\{S\}$ from Equation 2.9 into Equation 2.10 gives

$$\{S_D\} = -\mu \left[\frac{\dot{Q}}{|\dot{Q}|}\right] \{|[K^P]\{Q\}|\} \tag{2.11}$$

2.3 Water-Wave Medium

Several theories exist which analytically describe the kinematics of different type water waves. For a given set of conditions, water depth, wave height, etc., one theory is usually more accurate than the others and determining which is the most appropriate often presents a perplexing problem. If the Morison equation is used to define the wave's kinetics, drag and inertia coefficients based on the chosen theory are required, an important factor to consider when making the selection. Fortunately, interest in offshore activity has resulted in a concentrated effort to alleviate the problems associated with wave selection and wave-force computations.

Because of its inherent simplicity, and in many cases its ability to represent the kinematics of a variety of water waves, the Airy or linear wave theory is often used in the analysis of periodic wave problems; for these reasons it was selected for use in this investigation. It should be noted, however, that the numerical methods used to solve the differential equations of motion provide considerable flexibility in the selection of wave theories. For example, the same method of analysis can be applied to study the pile's response to waves described by the Stokes third order theory, Stokes fifth order theory, Solitary theory, and others. An extension of this study could quite feasibly amend the computer program to give the user an option in selecting the wave theory.

Morison's equation, which was applied in this study, defines the total force on a structure due to wave action as the resultant of an inertia force and a drag force. For a stationary cylinder the force per unit length in the horizontal direction f(z,t) at depth z and time t is given by:

$$f(z,t) = C_I \rho \frac{\pi D_z^2}{4} a(z,t) + \frac{1}{2} C_D \rho D_z v(z,t) \left| v(z,t) \right| \qquad (2.12)$$

where, C_I = inertia coefficient,

C_D = drag coefficient,

ρ = mass density of water,

D_z = diameter of cylinder at depth z,

$a(z,t)$ = water particle acceleration in horizontal direction at depth z and time t,

and

$v(z,t)$ = water particle velocity in horizontal directions at depth z and time t.

The inertia and drag coefficients are dependent on the pile's geometry, proximity effects of other piles or structures, surface roughness, and other conditions. Ippen (20) discusses factors which influence C_I and C_D and presents a summary of the results of various investigators who have attempted to define their values.

It is well known that C_D is a function of Reynolds number, R_n. Since R_n is a function of wave particle velocity, a time-dependent quantity, C_D, is seen to be time dependent. In determining values for C_D the following general ranges of R_n and the accompanying characteristics of C_D should be considered:

(1)	$0<R_n<$ 1,000	C_D varies with R_n
(2)	$1,000<R_n<1,000,000$	C_D approximately constant
(3)	$R_n>1,000,000$	C_D varies with R_n

For pile dynamic studies the first range can normally be neglected because particle velocities are small and consequently the drag component of Equation 2.12 is negligible in comparison with the inertia component. Values of R_n for offshore piles, subjected to design waves, usually encompass the second and third ranges. For example, the maximum value of R_n is approximately 5,000,000 for a 6-foot diameter pile, with a smooth surface, subjected to a 40-foot

wave. Nevertheless, assuming the value of C_D in the second range is valid for all ranges results in a conservative analysis because C_D decreases after R_n enters the third range. It therefore appears reasonable to simplify the analysis by making this assumption, as has been done in this study.

Since most offshore piles exhibit a certain degree of flexibility, Equation 2.12 must be modified to include interactive effects between the pile and the wave. With reference to Figures 2.1 and 2.3 and Equation 2.12, if $f_i(t)$ is the horizontal force on the pile per unit length at node i,

$$f_i(t) = K_{iI}[a_i(t) - \ddot{Q}_{i,1}(t)] + K_{iD}[v_i(t) - \dot{Q}_{i,1}(t)]\left|[v_i(t) - \dot{Q}_{i,1}(t)]\right| \qquad (2.13)$$

where

$$K_{iI} = C_I \rho \frac{\pi D_i^2}{4},$$

$$K_{iD} = \frac{1}{2} C_D \rho D_i,$$

$\ddot{Q}_{i,1}(t)$ and $\dot{Q}_{i,1}(t)$ = absolute horizontal acceleration and velocity, respectively, of the pile at node i at time t,

and

$a_i(t)$ and $v_i(t)$ = absolute horizontal particle acceleration and velocity, respectively, at node i at time t.

Expressions for the water particle velocity and acceleration, according to Airy or small-amplitude theory, are given in Equations 2.14 and 2.15. Reference should be made to Figure 2.5 for parameter definitions.

$$v_i(t) = \frac{H}{2}\sigma \frac{\cosh\beta(h+z_i)}{\sinh \beta h}\cos(\beta x-\sigma t) \tag{2.14}$$

$$a_i(t) = -\frac{H}{2}\sigma^2 \frac{\cosh\beta(h+z_i)}{\sinh \beta h}\sin(\beta x-\sigma t) \tag{2.15}$$

In these expressions,

z_i = distance from SWL (still water level) to node i (note that z_i is negative if node i is below SWL),

σ = wave angular frequency = $\frac{2\pi}{T}$,

β = wave number = $\frac{2\pi}{\lambda}$

where T is the wave period and λ the wave length. Also note that the origin of $(\beta x-\sigma t)$ is located at the wave crest.

For simplicity, the pile is assumed to be located at x = 0. Noting that

$$r_i = h + z_i \tag{2.16}$$

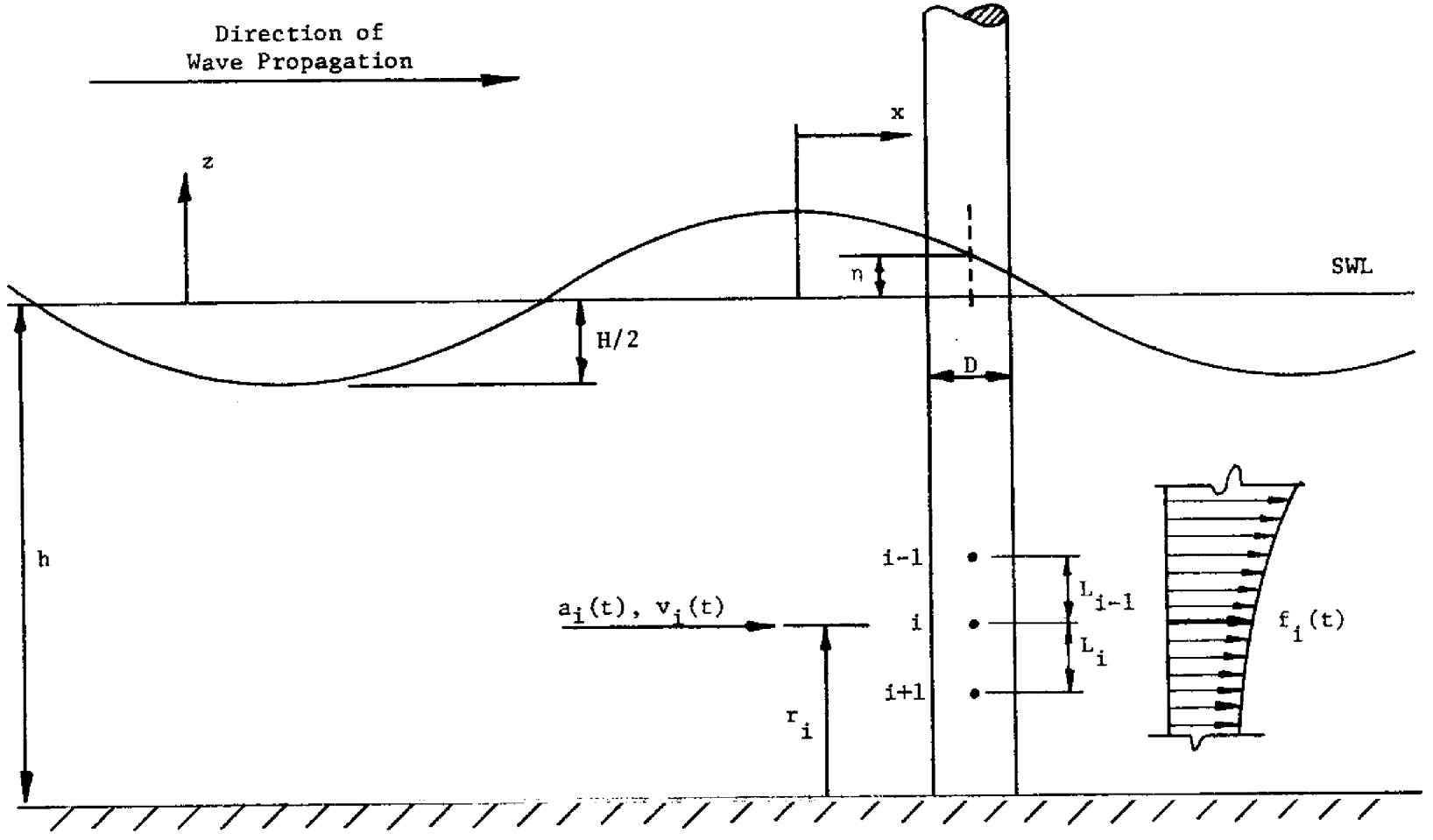

FIGURE 2.5 - WAVE DEFINITION SKETCH (AIRY THEORY)

Equations 2.14 and 2.15 can be rewritten as

$$v_i(t) = \frac{H}{2}\,\sigma\,\frac{\cosh\beta r_i}{\sinh\,\beta h}\cos\sigma t \qquad (2.17)$$

$$a_i(t) = -\frac{H}{2}\,\sigma^2\,\frac{\cosh\beta r_i}{\sinh\beta h}\sin\sigma t \qquad (2.18)$$

The expression for the instantaneous vertical displacement of the water surface above or below SWL is given by η, where

$$\eta = \frac{H}{2}\cos\,\sigma t \qquad (2.19)$$

For compatibility with the discrete parameter system selected for the pile, the distributed force of the wave must be resolved into a series of concentrated nodal loads. Referring to Figure 2.5, the concentrated force on node i is given by $F_i(t)$, where

$$F_i(t) = f_i(t)[0.5(L_{i-1} + L_i)] \qquad (2.20)$$

As seen in Equations 2.17 and 2.18, particle velocities and accelerations at a given time t vary exponentially with the vertical position along the pile, r_i. It follows from Equation 2.13 that $f_i(t)$ varies in a similar manner, and that its rate of change increases as r_i increases. Consequently, discretion must be exercised in selecting the spacing between the nodes, especially along the length of the pile immediately above and below SWL where the rate of change of $f_i(t)$ is greatest, so that large errors are not introduced by the linear assumption inherent in Equation 2.20.

Letting

$$L_{ie} = 0.5(L_{i-1} + L_i) \tag{2.21}$$

and by use of Equation 2.13, Equation 2.20 can be rewritten as

$$F_i(t) = K_{iI}L_{ie}[a_i(t) - \ddot{Q}_{i,1}(t)] + K_{iD}L_{ie}[v_i(t) - \dot{Q}_{i,1}(t)] \left| [v_i(t) - \dot{Q}_{i,1}(t)] \right| \tag{2.22}$$

In matrix notation, the concentrated nodal forces may be written as

$$\{F(t)\} = \begin{Bmatrix} F_1(t) \\ F_2(t) \\ \cdot \\ \cdot \\ \cdot \\ F_j(t) \end{Bmatrix} \tag{2.23}$$

2.4 Soil Medium

Previous investigators have used many types of rheological models to describe the static and dynamic behavior of soil; and although many of these models have met with a certain degree of success, no particular one has been generally accepted for all cases. Some of this can no doubt be attributed to the diverse nature of the problems undertaken.

The idealized discrete model selected to represent the dynamic properties of the laterally loaded soil and its force-displacement characteristics are shown in Figure 2.6. A similar model has been

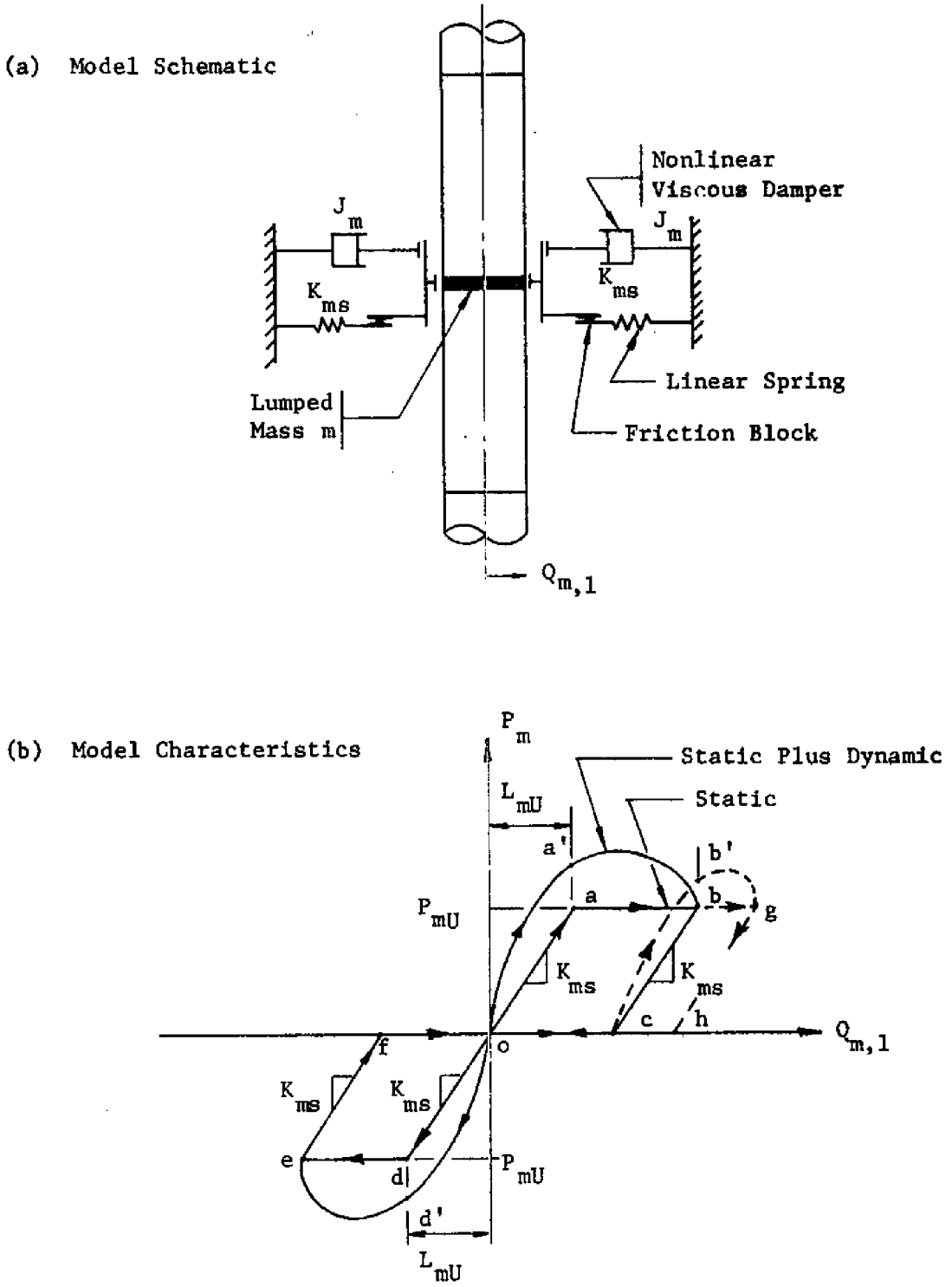

FIGURE 2.6 - SOIL RHEOLOGICAL MODEL AT NODE m

used successfully in describing the vertical response of piles during driving (23,36,38) and in describing the lateral response of piles during seismic loading (31). A model of this type was placed on both sides of each node along the length of pile between the water-soil interface and the pile's base (nodes j through n in Figure 2.1). Interaction between soil elements was assumed negligible, i.e., it was assumed that deformation of one soil element did not change the properties of the others. This is commonly called the Winkler assumption.

Figure 2.6(b) depicts the force-displacement properties of the model in two forms, its resistance to slowly applied deformations ("static" curve) and its resistance to dynamically applied deformations ("static plus dynamic" curve). In the static case, the soil's resistance at node m, P_m, is proportional to the pile's displacement $Q_{m,1}$, provided the displacement is less than or equal to L_{mU}. Any pile movement in excess of $\pm L_{mU}$ is met by a constant resistance, P_{mU}, the ultimate static load capacity of the soil at node m. Displacement beyond point a in Figure 2.6 also causes permanent set in the soil equal to the distance between points a and b, denoted as PPS_m (positive permanent set at node m). If permanent set occurs, the pile segment returns along bc, the slope of line bc assumed equal to oa. From point c to point o, whose length also equals PPS_m, the pile segment experiences no soil resistance due to the gap developed between the pile wall and soil.

As the segment moves slowly to the left of its undeformed position (negative direction), the soil's resistance characteristics are similar to those for positive displacements. In this case, NPS_m denotes the negative permanent set at node m and its value is equal to the distance de, or fo.

If, during the pile's response history, positive permanent set occurs at node m, the resistance of the soil as the segment returns to the right is traced by ocbgho and the permanent set would then equal to the distance ag. If negative permanent set occurs, the resistance would be of a similar nature.

The "static plus dynamic" curve represents the total soil resistance and equals the sum of the soil's spring resistance, and the viscous damping resistance. Its height above the "static" curve is a function of the rate at which the damper is deformed. As shown in Figure 2.6, it was assumed that the damper is active during increasing displacements only and consequently does not retard the pile's return toward the undeformed position.

Researchers (11) have demonstrated that the damping force in soil, P_{md}, can be described by use of the model shown in Figure 2.6 and Equation 2.24.

$$P_{md} = (P_{ms})(J_m)(\dot{Q}_{m,1})^{n_m} \tag{2.24}$$

where

P_{ms} = static resistance in soil spring

and

J_m and n_m = constants dependent on soil properties.

The term P_{ms} in Equation 2.24 is included to account for the quantity of soil being displaced at node m.

Expressions for the total soil resistance P_m at node m, during a typical displacement, defined by the path oa'bco in Figure 2.6b, are given by Equations 2.25 through 2.28.

From o to a':

$$P_m = P_{ms}[1 + (J_m)(\dot{Q}_{k,1})^{n_m}] \tag{2.25}$$

where

$$P_{ms} = (K_{ms})(Q_{m,1}) \tag{2.25a}$$

From a' to b:

$$P_m = P_{mU}[1 + (J_m)(\dot{Q}_{m,1})^{n_m}] \tag{2.26}$$

From b to c:

$$P_m = P_{ms} \tag{2.27}$$

where

$$P_{ms} = (K_{ms})(Q_{m,1} - PPS_m) \tag{2.27a}$$

From c to o:

$$P_m = o \tag{2.28}$$

Therefore, in general, Equations 2.29 are general equations for soil resistance at each node:

$$\{P\} = \{P_s\} + \{P_d\} \tag{2.29}$$

where

$$\{P_s\} = \{N_1\}\ [K_s]\{Q_1\} + [N_2]\ \{P_U\} + \{N_3\}\ [K_s]\{PPS\} \tag{2.30}$$

and

$$\{P_d\} = [N_4]\ \{P_s\}\ [J]\ \{\dot{Q}^n\} \tag{2.31}$$

The order of P is (n-j) by 1 (reference Figure 2.1). In Equations 2.30 and 31, values of the N's depend on the pile's position, direction of motion, and the amount of permanent set. With reference to Figure 2.6, for resistance at node m according to the path oa'bco, the N's have the following values:

range →	o to a'	a' to b	b to c	c to o
N_{m1} =	+1	0	+1	0
N_{m2} =	0	+1	0	0
N_{m3} =	0	0	-1	0
N_{m4} =	+1	+1	0	0

As another example, consider the resistance at node m according to ocb'gho, in which case

range →		o to c	c to b'	b' to g	g to h	h to o
N_{m1}	=	0	+1	0	+1	0
N_{m2}	=	0	0	+1	0	0
N_{m3}	=	0	-1	0	-1	0
N_{m4}	=	0	+1	+1	0	0

As the pile interacts with the soil, some quantity of soil is accelerated developing an inertia force which acts against the pile's motion. The actual quantity or "effective" mass of soil influenced by the motion is difficult to determine. Fortunately, however, these inertia forces are usually small compared to the soil's spring forces and the pile's elastic shear forces and can be neglected (22). The effective soil mass was assumed negligible in this analysis.

The pile also experiences some rotational restraint and rotational damping from the soil. These effects are usually negligible also when compared with their lateral counterpart.

Another assumption inherent in the proposed soil model is that creep effects in the soil are of secondary importance. It is recognized that with repeated loads from waves of varying magnitude the soil characteristics will be in a continual state of flux and may be influenced to some extent by the degree of creep that occurs. However, the computer time required for such an analysis would be prohibitive, so the method of analysis proposed herein is applicable for determining the response of a pile over relatively short periods

of time only. During short time periods it is doubtful that creep effects will significantly influence the pile's response. This time limitation will not restrict the applicability of the method provided the soil characteristics are definable at the beginning of the time period under analysis.

2.5 Equations of Motion

An idealization of the entire system is illustrated in Figure 2.7. In general, for the planar case, each node or lumped mass has three degrees of freedom. Thus a system having n nodes would have 3(n) degrees of freedom. For small displacements the vertical motion of the pile is independent or uncoupled from rotational and horizontal motion, as assumed. Since the excitation forces under consideration result in lateral and rotational motion only, the number of degrees of freedom of interest reduces to 2(n).

In formulating the equations of motion it was further assumed that the rotational inertia of each lumped mass and the structural damping of the pile associated with the rotational displacements were negligible when compared to their lateral counterparts. These assumptions together with previously mentioned assumptions regarding the soil's rotational restraint in effect reduced the number of equations of motion necessary to define the pile's response to n and permit the use of a "reduced" pile stiffness matrix. With reference to Equation 2.9, $[K^P]$ can be written as

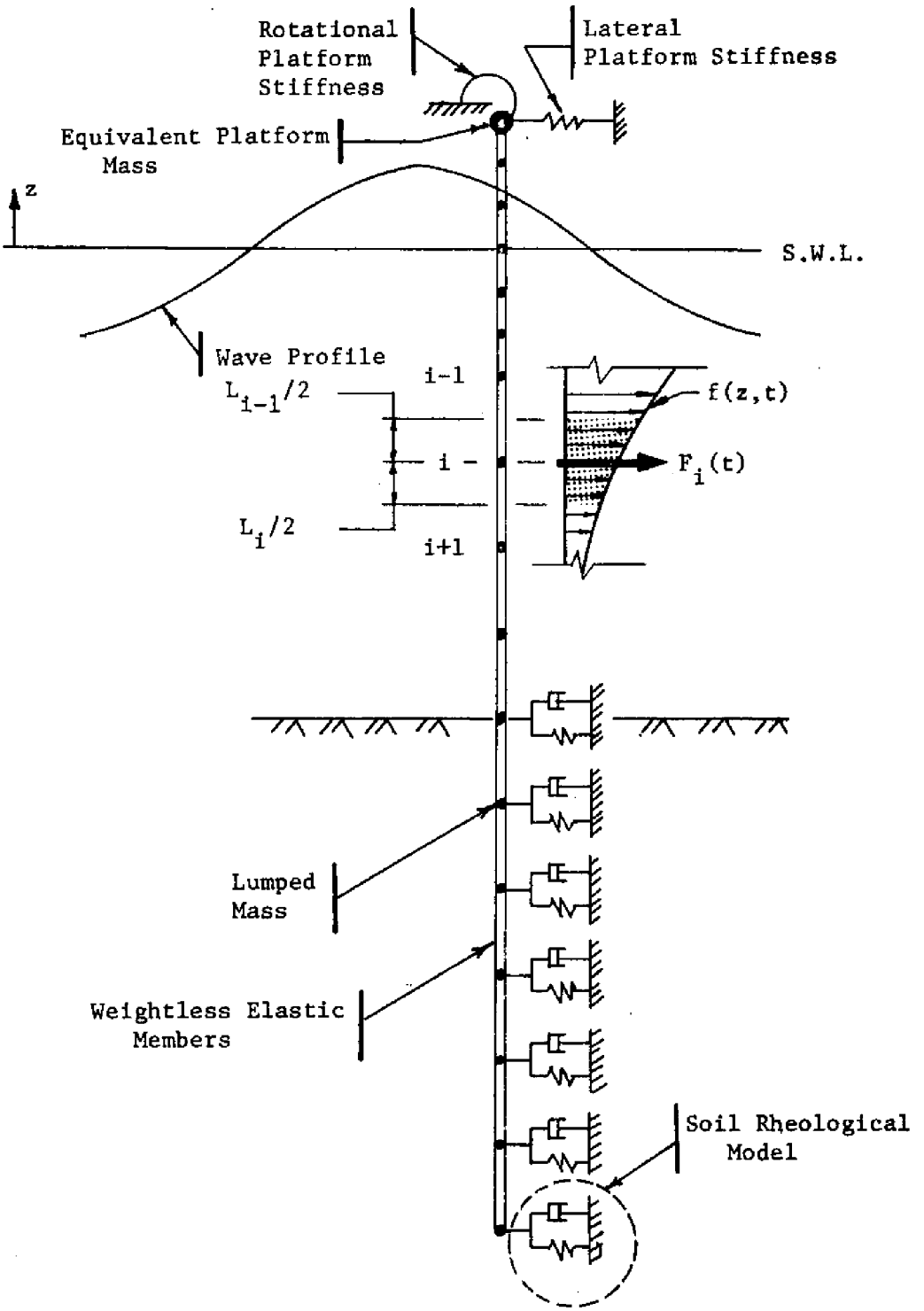

FIGURE 2.7 - SYSTEM IDEALIZATION

$$[K^p] = \begin{bmatrix} K_U^p & \\ & K_S^p \end{bmatrix} \tag{2.32}$$

where $[K_U^p]$ is the portion due to vertical displacements $\{Q_{i,2}\}$, which are of no relevance, and $[K_S^p]$ is the portion due to lateral and rotational displacements, $\{Q_{i,1}\}$ and $\{Q_{i,3}\}$, respectively. By partitioning, $[K_S^p]$ can be written as

$$[K_S^p] = \begin{bmatrix} \alpha_{LL} & \alpha_{LR} \\ \alpha_{RL} & \alpha_{RR} \end{bmatrix} \tag{2.33}$$

where

$[\alpha_{LL}]$ = matrix of stiffness coefficients which relate lateral displacements to lateral loads, all other displacements being zero;

$[\alpha_{LR}]$ = matrix of stiffness coefficients which relate rotational displacements to lateral loads, all other displacements being zero;

$[\alpha_{RL}] = [\alpha_{LR}]^T$;

and

$[\alpha_{RR}]$ = matrix of stiffness coefficients which relate rotational displacements to rotational loads, all other displacements being zero.

From the assumptions regarding the rotational degress of freedom, the pile's elastic resistance $\{S_L\}$ to lateral displacements $\{Q_{i,1}\}$ is given by

$$\{S_L\} = [K_R^P]\ \{Q_{i,1}\} \tag{2.34}$$

and the structural damping $\{S_{DL}\}$ in the pile is given by

$$\{S_{DL}\} = -\mu\left[\frac{\dot{Q}_{i,1}}{|\dot{Q}_{i,1}|}\right] |[K_R^P]\{Q_{i,1}\}| \tag{2.35}$$

where

$$[K_R^P] = [\alpha_{LL}] - [\alpha_{LR}][\alpha_{RR}]^{-1}[\alpha_{LR}]^T \tag{2.36}$$

Through this reduction procedure the nodes are allowed to rotate and move laterally but only n equations of motion are needed to describe the pile's motion, where the n unknown are the lateral displacements at the nodes.

To simplify notation, the lateral displacements $\{Q_{i,1}\}$ will henceforth be denoted as $\{Q_i\}$. The equations of motion are given by Equation 2.37.

$$\left[\begin{array}{cc} M_T^P & 0 \\ \hline 0 & M_B^P \end{array}\right]\left\{\begin{array}{c} \ddot{Q}_{i,T} \\ \hline \ddot{Q}_{i,B} \end{array}\right\} + \left\{\begin{array}{c} 0 \\ \hline P \end{array}\right\} + \left\{\begin{array}{c} S_{L,T} \\ \hline S_{L,B} \end{array}\right\} + \left\{\begin{array}{c} S_{DL,T} \\ \hline S_{DL,B} \end{array}\right\} = \left\{\begin{array}{c} F(t) \\ \hline 0 \end{array}\right\} \tag{2.37}$$

Each term in Equation 2.37 has been defined previously. For convenience, the equations have been partitioned, with the subscript "T" referring to degrees of freedom above the ocean bottom and "B" referring to those below the ocean bottom. This procedure permits efficient utilization of computer storage space in the solution process.

CHAPTER III

NUMERICAL SOLUTION TECHNIQUES

3.1 General

To solve the second order nonlinear differential equations of motion of the system, three different numerical integration schemes were attempted, namely, a recursion method, Milne's predictor-corrector method, and the fourth-order Runge-Kutta method.

Recursion method. An effort was made to develop suitable recurrence equations by substituting various finite difference formulas for their equivalent in the equations of motion. However, due to the degree of nonlinearity of the problem this approach met with little success.

Milne's predictor-corrector method. This method can be used to solve higher-order equations of the type found in this study and the procedural steps for its application can be found in most "numerical methods" books. Basically, as related to this study, an integration formula employing four previously known points (sometimes called an "open integration formula") was applied at point i-1 to predict the value of Q at point i, denoted as $(Q_i)_p$. The corrected value $(Q_i)_c$ was obtained by using the predicted value in a form of the well known "Simpson's" one-third rule (which, in this form would be called a "closed integration formula"). Greater accuracy was obtained by iterating the procedure, an advantage of

this method since it permits one to place a lower bound on the truncation error. Greater accuracy can also be realized by reducing the integration interval.

The most evident disadvantage of this method is the requirement that some starting procedure must be used to obtain the first four values of node displacements and velocities. The Runge-Kutta scheme can be and was used to determine these starting values. Another disadvantage is that changes in the interval of integration are difficult to make during the solution process.

Runge-Kutta method. A description of this method and the procedural steps needed to employ it are also available in most numerical analysis books and will not be given here. There are different order formulas associated with the Runge-Kutta methods; the fourth order formulas were used in this analysis. In essence, the procedure employs forward integration formulas with known values at point i-1 to estimate Q_i and $\dot{Q}_i$.

It was tried because of its proven suitability to nonlinear differential equations of the type found herein. In contrast with Milne's predictor-corrector method the integration interval can be changed at any time without difficulty, and it is self starting. Its major disadvantage is that it is rather difficult to estimate errors.

3.2 Summary

Since an adequate recursion equation could not be developed, the choice of a solution method was reduced to Milne's predictor-corrector method or the Runge-Kutta method.

Milne's method without iteration and the fourth-order Runge-Kutta method have the same truncation error, of order $(\Delta t)^5$, Δt being the interval of integration. Outwardly, it would appear that Milne's method would reach a solution in half the time required by the Runge-Kutta method since the former requires roughly one-half the number of calculations in one interval of integration. This was not found to be the case. In fact, Milne's method required approximately twice the time of Runge-Kutta to converge on the solution. Specific reasons cannot be given for this occurrence but it is known (24) that Milne's method is likely to be unstable, which could account for the additional time required.

Another factor of importance in numerical solutions of differential equations is what the writer chooses to call the "instability rate" of the solution process. If $(\Delta t)_c$ represents the critical interval of integration or the maximum value of Δt for which the solution is stable, any value in excess of $(\Delta t)_c$ will result in a divergence of the solution. The rate of divergence as a function of the amount of excess in $(\Delta t)_c$ is defined as the instability rate. The Runge-Kutta method exhibited a high

instability rate, an advantageous feature since large amounts of computer time are not required to determine $(\Delta t)_c$.

Also worth mentioning is the observation that values of $(\Delta t)_c$ in the Runge-Kutta method appeared to be insensitive to the initial conditions or the external excitation forces on the system. Rather, values of $(\Delta t)_c$ exhibited a dependence on the characteristics of the system itself, i.e., its mass and stiffness.

Based on these findings the fourth-order Runge-Kutta method was selected as the more appropriate of the methods investigated.

CHAPTER IV

VALIDATION STUDY

4.1 General

An absence of experimental data on the lateral response of full-scale offshore piling precluded a conclusive validation of the method of analysis presented. Nevertheless, there were available certain mathematical solutions and experimental tests which could be used to determine the validity of the model to a great extent.

4.2 Analytical Study

Prior to studying the mathematical model's response with actual or experimental cases, a simple analytical study was undertaken. Its purpose was to check out the accuracy of the model, the numerical solution scheme, and the computer coding.

Figure 4.1 shows the idealized elastic model used in the analysis. The distributed weight, w, of the structure was lumped at the node points shown and a concentrated weight of 63 pounds was added to node 1. The procedure employed was to first determine the fundamental frequency and mode shape of the structure by employing a well known method for obtaining eigenvalues, the Stodola-Vianello iteration procedure. Next, as initial conditions, the structure was displaced laterally into a fundamental mode shape, released with no initial velocity, and allowed to vibrate freely, with the

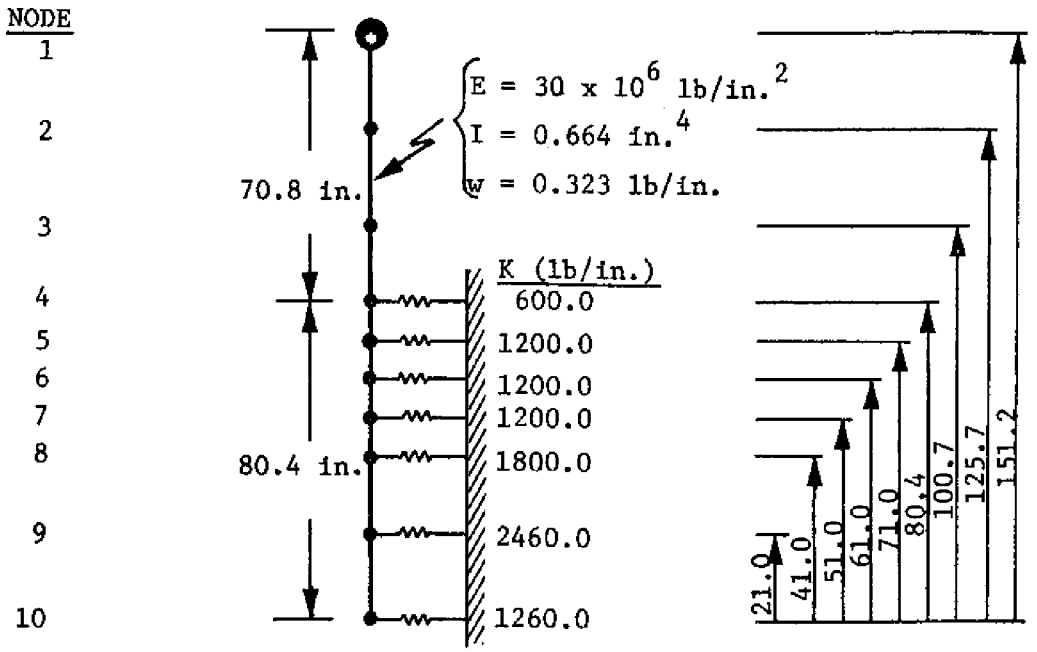

FIGURE 4.1 - ELASTIC MODEL

TABLE 4.1 - ELASTIC MODEL COMPARISONS

Node	Nodal Displacement (in.)	
	Theoretical	Computed[a]
1	1.0000	0.9995
2	0.6341	0.6336
3	0.3147	0.3145
4	0.1236	0.1236
5	0.0601	0.0602
6	0.0184	0.0185
7	-0.0058	-0.0057
8	-0.0174	-0.0174
9	-0.0196	-0.0197
10	-0.0119	-0.0119

[a]After three complete cycles.

response being determined by the Runge-Kutta method described previously. The computed response of the structure is shown in Table 4.1 along with the theoretical values. These are the lateral nodal displacements after three complete cycles, with node 1 being the top node and the others numbered consecutively downward. As seen, the Runge-Kutta method is highly accurate in this case. The fundamental frequency was computed as 2.95 cycles per second by the iteration method and 2.94 cycles per second by the Runge-Kutta method.

4.3 Structural Damping Study

The range of values for the structural damping factor, μ, of steel structures was found to be large. A test program was therefore conducted to determine μ for the steel pipes used in the experimental validation studies.

A 2 inch standard pipe, 13 feet in length, was instrumented so that stresses could be measured as the pipe was allowed to vibrate. One end of the pipe was fixed and the other end displaced and then released. A record of stresses with time as the pipe vibrated was then taken and the logarithmic decrement of the response determined. The percent of critical damping was found to be 2.5 percent.

To relate percent of critical damping to the structural damping factor, μ, an analytical study was performed. A value of μ equal to 0.015 was assumed for the structure shown in Figure 4.1 and the

response computed as the structure vibrated freely. This value of μ resulted in a 0.5 percent of critical damping. This procedure was repeated for other values of μ and the results are shown plotted in Figure 4.2 From the plot it is seen that a value of μ equal to 0.079 is needed to obtain 2.5 percent of critical damping.

4.4 Model Pile Studies

To obtain a measure of the mathematical model's accuracy in simulating field conditions, field tests of model piles were conducted. Three different size standard steel pipes were embedded in a clay soil having a fairly constant composition with depth. The test site was located just west of the northern end of the western most north-south runway at the Texas A&M Research Annex. Since other researchers (35) have made laboratory tests of the soil at this site and have documented its properties, no description is given here. Shown in Figure 4.3 is the configuration of the embedded pipes, while Table 4.2 lists their dimensions and mechanical properties.

Two basic types of tests were made on each pipe, static and dynamic, and a description of each follows.

Static tests. Before performing the dynamic tests, static lateral load tests were made. Figure 4.4 gives the results of the 2.0 inch pipe test and shows the manner in which the load was applied. For the 2.0 inch pipe the relationship between load and deformation is seen to be approximately constant, as was also

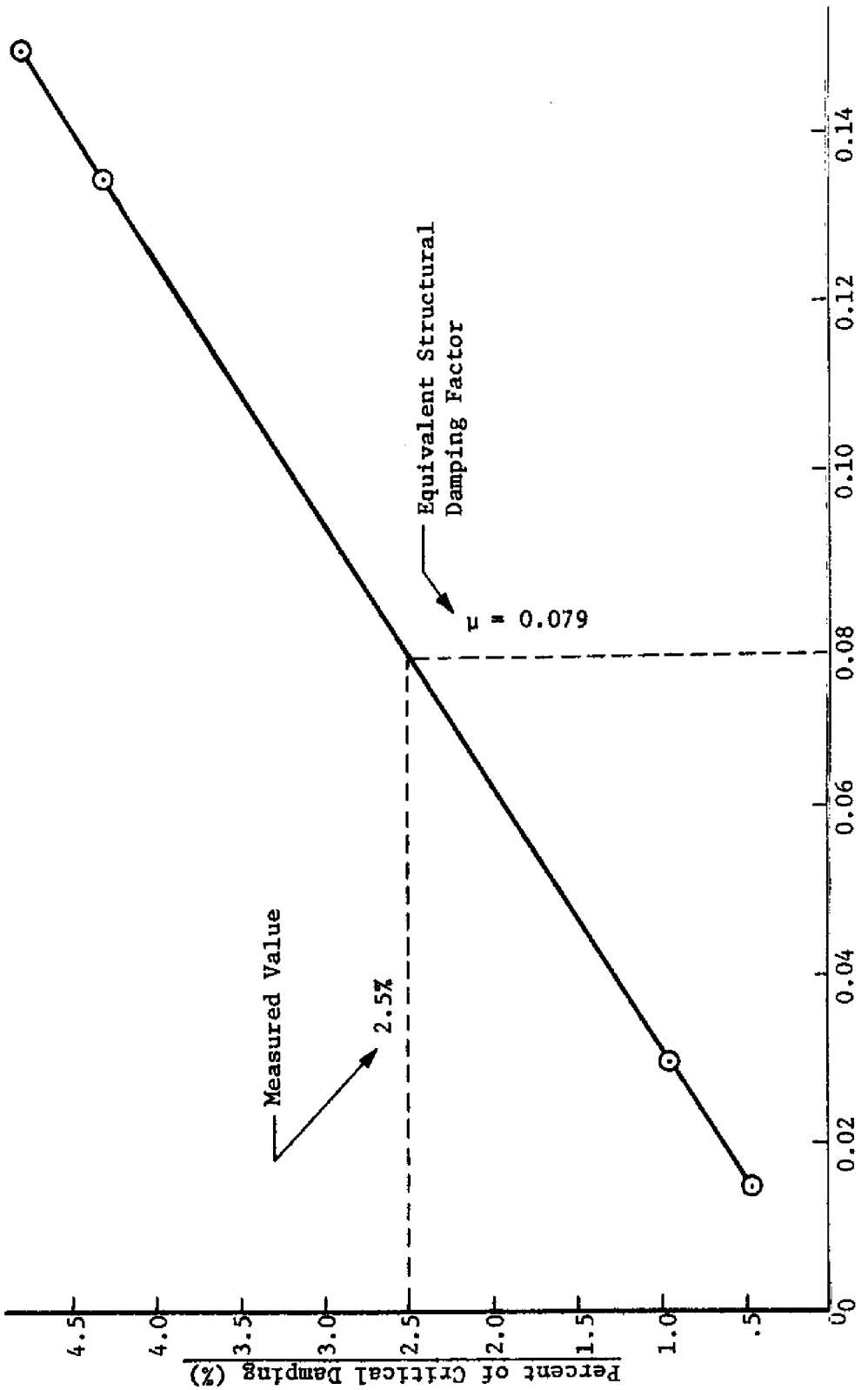

FIGURE 4.2 - RELATION BETWEEN STRUCTURAL DAMPING AND CRITICAL DAMPING

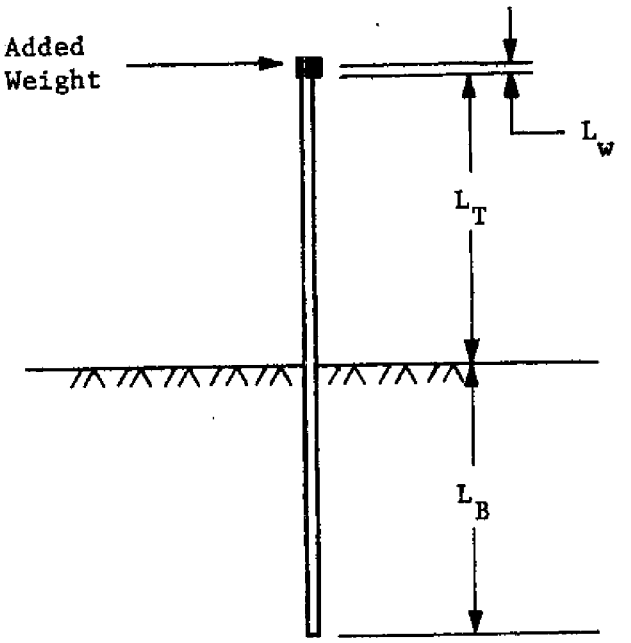

FIGURE 4.3 - PIPE CONFIGURATION

TABLE 4.2 - PIPE DIMENSIONS AND PROPERTIES

Nominal I.D.(in.)	L_B (in.)	L_T (in.)	L_w (in.)	Wt/ft (lb/ft)	I_4 (in.^{4})	Added Wt (lb)
1.5	81.0	67.0	7.0	2.72	0.308	63.0
2.0	80.4	67.5	3.3	3.65	0.664	63.0
3.0	63.0	89.0	4.5	7.58	3.000	66.0

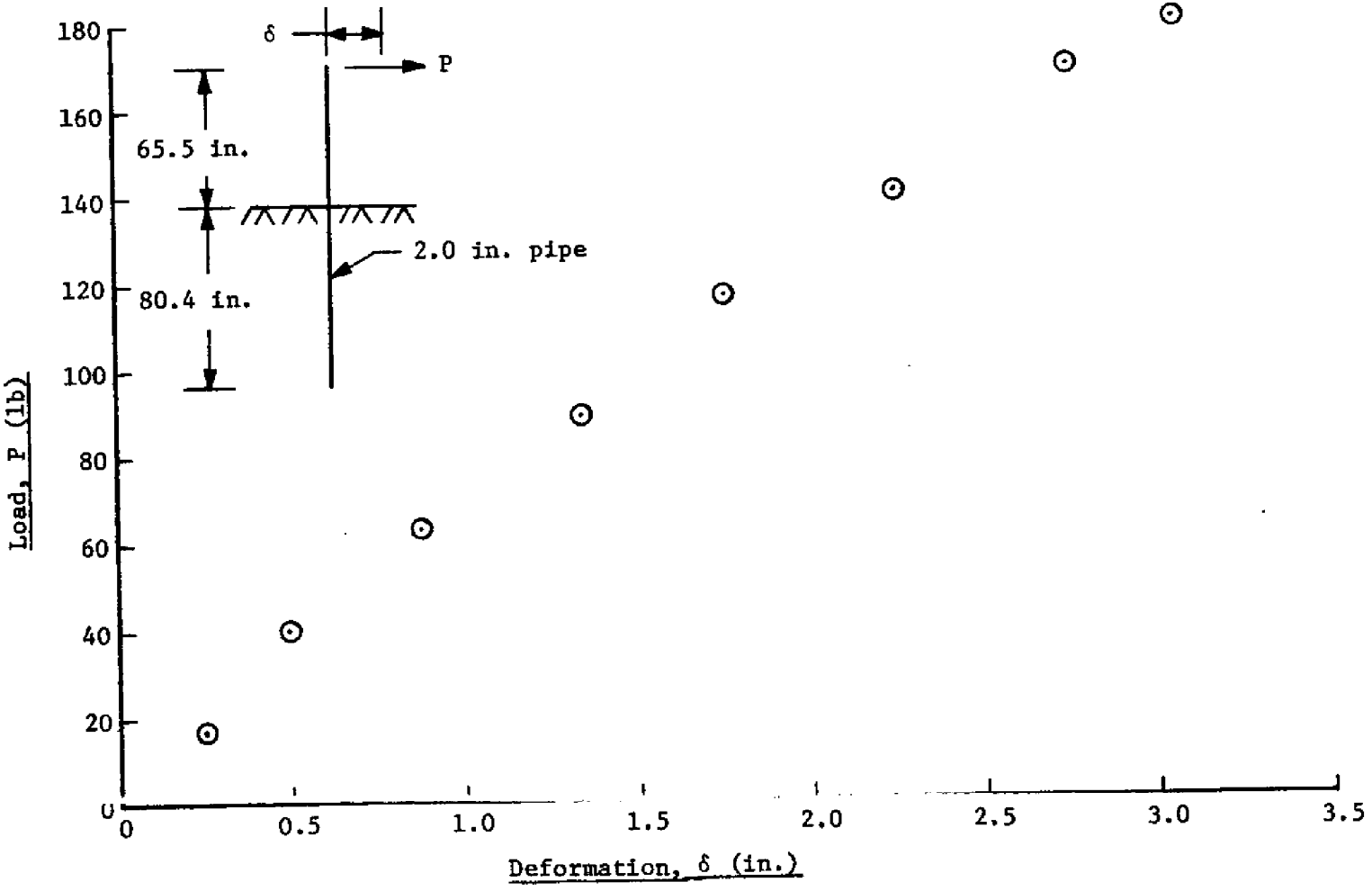

FIGURE 4.4 - LOAD DEFORMATION RESULTS, 2.0 INCH PIPE

observed for the 1.5 inch and the 3.0 inch tests, indicating that the soil and pipe material remain approximately in the linearly elastic range. Some soil failure appeared to have occurred, however, at and just below the soil surface after the deformation at the top of the pipe reached 2.75 inches. Table 4.3 lists the slope of the P-δ curve for each of the three pipe tests.

TABLE 4.3 - STATIC LOAD DATA

Pipe Size (in.)	Slope of P-δ Curve (lb/in.)
1.5	28.0
2.0	60.0
3.0	225.0

Dynamic tests. Free vibration tests were made on all three pipes. A Stathem accelerometer, model number F-20-350, located at the top of each pipe, measured acceleration with time after the pipes were given an initial displacement and then released. Accelerations were recorded on a Honeywell 1508 visicorder oscillograph. To prevent the accelerations and frequencies of vibration from exceeding the accelerometer limits, a concentrated weight of 63 pounds was attached to the top of the 1.5 and 2.0 inch pipes, and a weight of 66 pounds was attached to the top of the 3.0 inch pipe. Results of these tests are discussed in the following section.

4.5 Comparison of Field Tests with Model Predictions

Each idealized pipe used in simulating the test pipes consisted of 10 lumped masses. Figure 4.5 shows the manner in which the pipes were idealized and Table 4.4 lists information pertinent to each configuration, including soil stiffnesses used in the analysis. Concentrated weights equal to that of the field tests (reference Table 4.2) were added to node 1.

Although a considerable number of laboratory tests had been performed on the soil from the test site, data which could be used to determine the variation of soil modulus of subgrade reaction with depth was not readily available. To make this determination an attempt was made to find a soil modulus which satisfied the measured static and dynamic data. The 2.0 inch pipe configuration was used in the analysis and the steps in the method employed were as follows:

1. Three different variations of the soil modulus of subgrade reaction with depth were assumed, viz., a triangular distribution, a trapezoidal distribution, and a constant distribution. These are shown as cases (a), (b), and (c), respectively, on Figure 4.6.
2. For each variation in step 1, the magnitude of the modulus was varied to determine the effect on the deflection at the top of the pipe. The lateral load at the top of the pipe was set at 100 pounds in each case and the pipe and

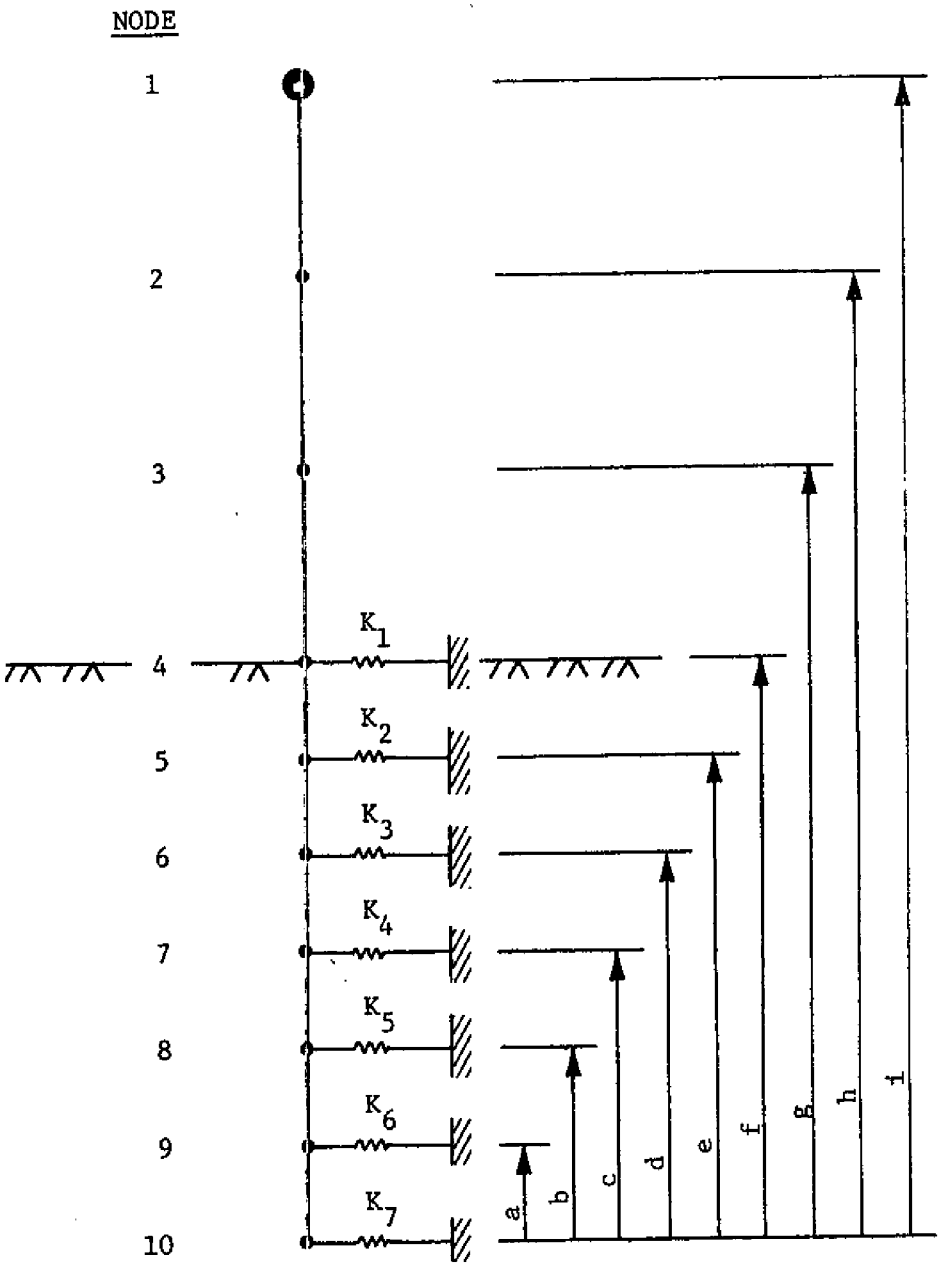

FIGURE 4.5 - GENERAL PIPE IDEALIZATION

TABLE 4.4 - IDEALIZED PIPE DATA

Pipe Size I.D. (in.)	Dimensions[a] (in.)								
	a	b	c	d	e	f	g	h	i
1.5	21.0	41.0	51.0	61.0	71.0	81.0	101.3	126.3	155.0
2.0	21.0	41.0	51.0	61.0	71.0	80.4	100.7	125.7	151.2
3.0	13.0	23.0	33.0	43.0	53.0	63.0	97.0	131.0	156.5
	Soil Stiffnesses[a] (lb/in.)								
	K_1		K_2	K_3	K_4	K_5	K_6	K_7	
1.5	214.0		482.0	533.0	587.0	959.0	1528.0	898.0	
2.0	267.0		602.0	666.0	734.0	1199.0	1910.0	1122.0	
3.0	394.0		912.0	1037.0	1161.0	1287.0	1625.0	1024.0	

[a]Reference Figure 4.5

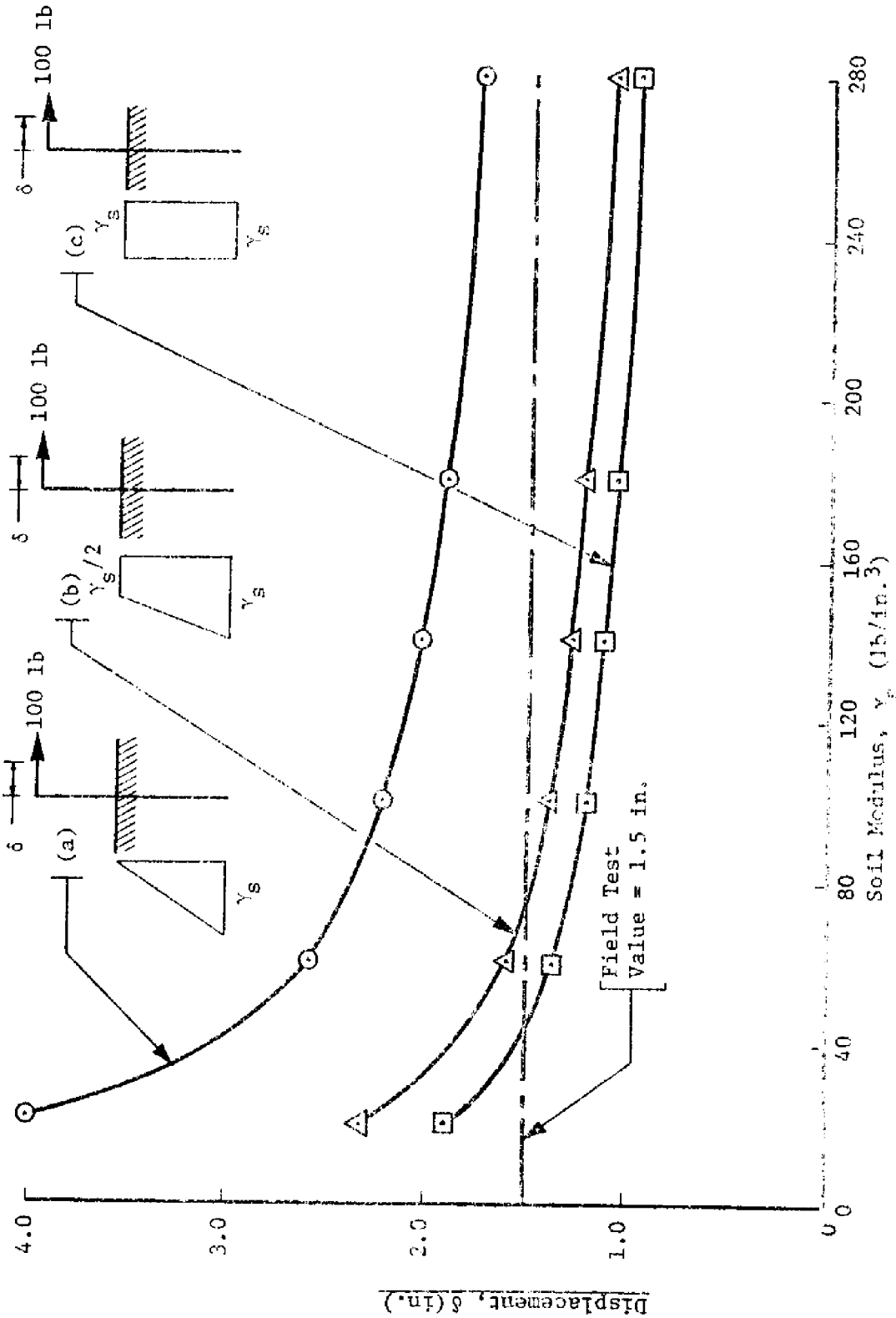

FIGURE 4.6 - DISPLACEMENT VERSUS SOIL MODULUS, 2.0 INCH PIPE

soil material were assumed to remain linearly elastic. Deformations were determined by use of the idealized model of Figure 4.5 and a finite-element computer program developed by the writer.

3. From the data generated in step 2, three curves were drawn, depicting deformations at the pipe's top versus magnitude of subgrade modulus γ_s. These curves are shown in Figure 4.5.
4. For each type of variation in step 1, the magnitude of the modulus was varied to determine the effect on the fundamental frequency of the idealized pipe-soil system. Again, a finite-element computer program, developed by the writer, was used for this purpose.
5. From the data generated in step 4, three curves were drawn, depicting fundamental frequency versus magnitude of subgrade modulus for the three variations described in step 1. These curves are shown in Figure 4.7.
6. The field test values were then superimposed on each graph, with a value of 1.5 inches being measured in the static load test and a frequency of approximately 2.5 cycles per second being measured in the dynamic test.

The triangular distribution was eliminated as a possibility since an unreasonably large value of γ_s would be required to satisfy the measured static value. Based on the static analysis (reference Figure 4.6), a value of γ_s equal to 44 appeared appropriate for

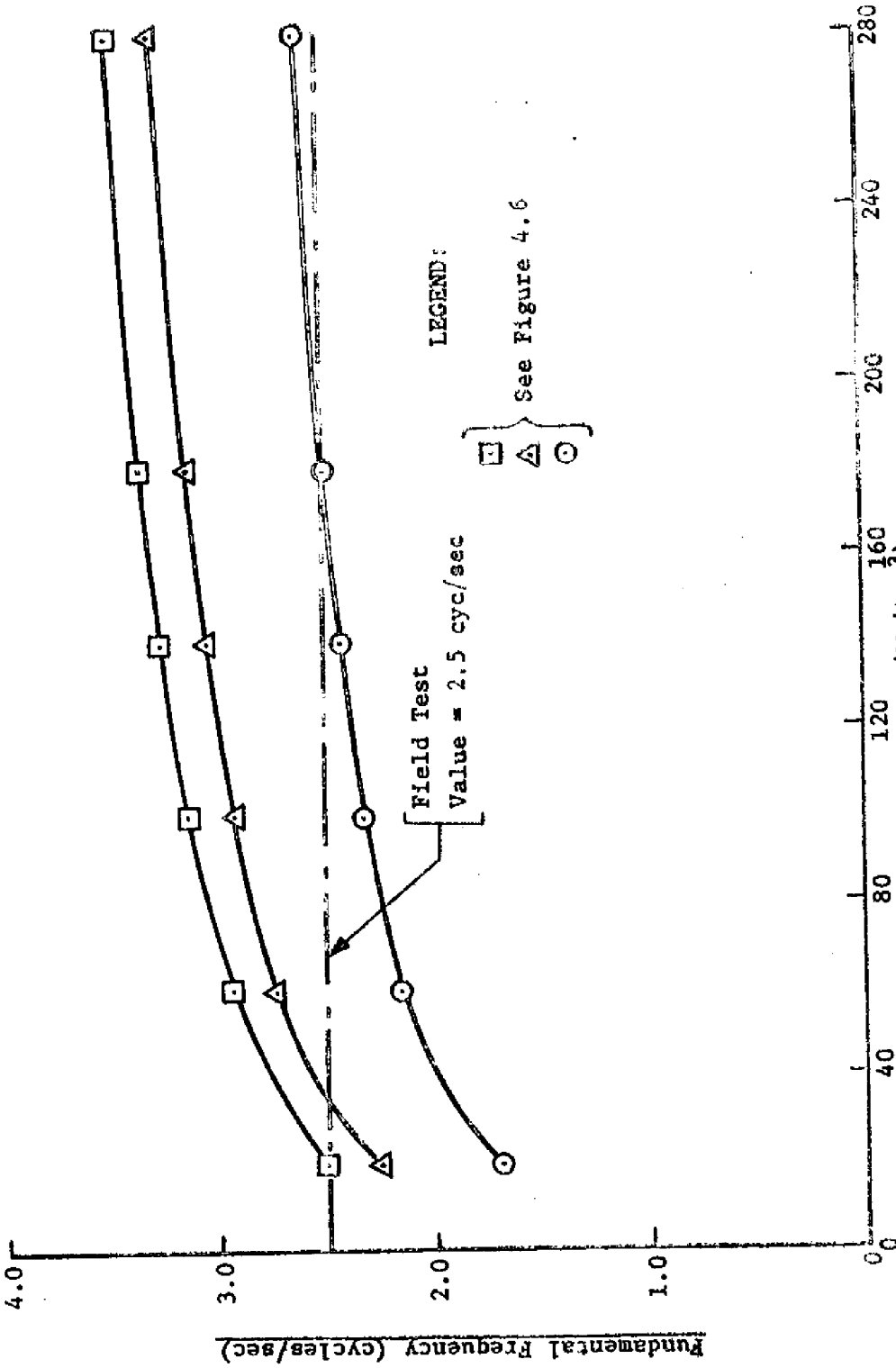

FIGURE 4.7 - FUNDAMENTAL FREQUENCY VERSUS SOIL MODULUS, 2.0 INCH PIPE

case (c) and γ_s equal to 75 for case (b). Based on the dynamic analysis (reference Figure 417), γ_s equal to 20 appeared appropriate for case (c) and γ_s equal to 35 for case (b). The correct value of γ_s seemed to lie between 20 and 75 and therefore a value of 45 ($lb/in.^3$) was tried in the simulation studies of all three pipe configurations. The values of soil stiffness listed in Table 4.4 are based on this value, with case (b) utilized as the type of distribution. This magnitude and variation of subgrade modulus is in general agreement with in situ measurements of a similar type soil (12).

Soil damping parameters were obtained from data acquired in prior laboratory studies (11). With reference to Equation 2.24, n_m for a "highly plastic" clay was found to be approximately 0.18. For the clay which best resembled that found at the test site, designated as EA 50 in the referenced report, the damping factor J_m was found to be approximately 0.9 seconds per foot, or 0.575 seconds per inch for velocities in inches per second. These values of n_m and J_m were assumed applicable along the entire embedded length of all three pipe configurations.

Studies made by Gill (12) were used to determine the value of L_{mU}, the deformation at which the soil's properties transit from elastic to plastic. After reviewing his experimental results, a value of 0.2 inches was decided upon for the entire embedded length of each pipe.

One other parameter had to be determined before the dynamic analysis could proceed, that being a determination of the initial displacement of each node of each pipe configuration. The only displacement measured in the field tests was that at the top of each pipe just prior to release. Analytical means were thus necessary to define the initial displacement at the other 9 nodes. A finite-element computer program developed by the writer was used for this purpose. Since it was written for a linearly elastic structure, a trial and error scheme was necessary to determine the desired displacements. Results of this analysis indicated that soil failure had occurred at node 4 of the 3.0 inch pipe, and at nodes 1 and 2 of both the 2.0 and 1.5 inch pipes. These results were confirmed by observations made by the writer during the field tests and consequently confirm to some extent the assumption made regarding L_{mU}.

Shown in Figures 4.8, 4.9, and 4.10 are the results of the simulation and field test studies. The acceleration at the top of each pipe versus time is plotted and, in general, good agreement between test and simulation values exist.

Predicted and experimental frequencies were in reasonable agreement, with the predicted value being slightly low in the 3.0 and 1.5 inch pipes and slightly high in the 2.0 inch pipe. Regarding the amount of damping, simulation results exhibited excess damping in the 3.0 inch pipe, insufficient damping in the 2.0 inch pipe, and approximately the correct amount in the 1.5 inch

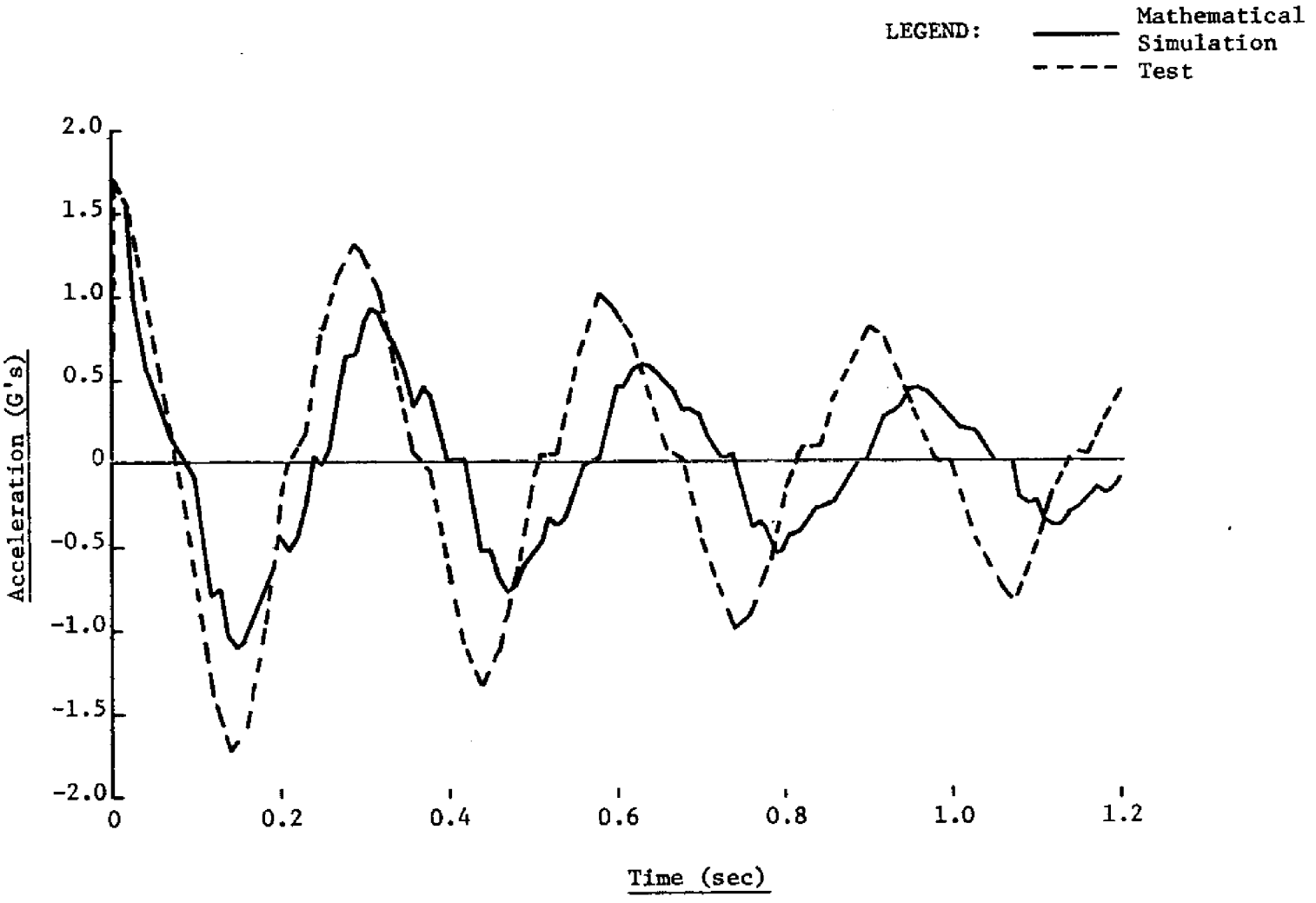

FIGURE 4.8 - ACCELERATION VERSUS TIME, 3.0 INCH PIPE

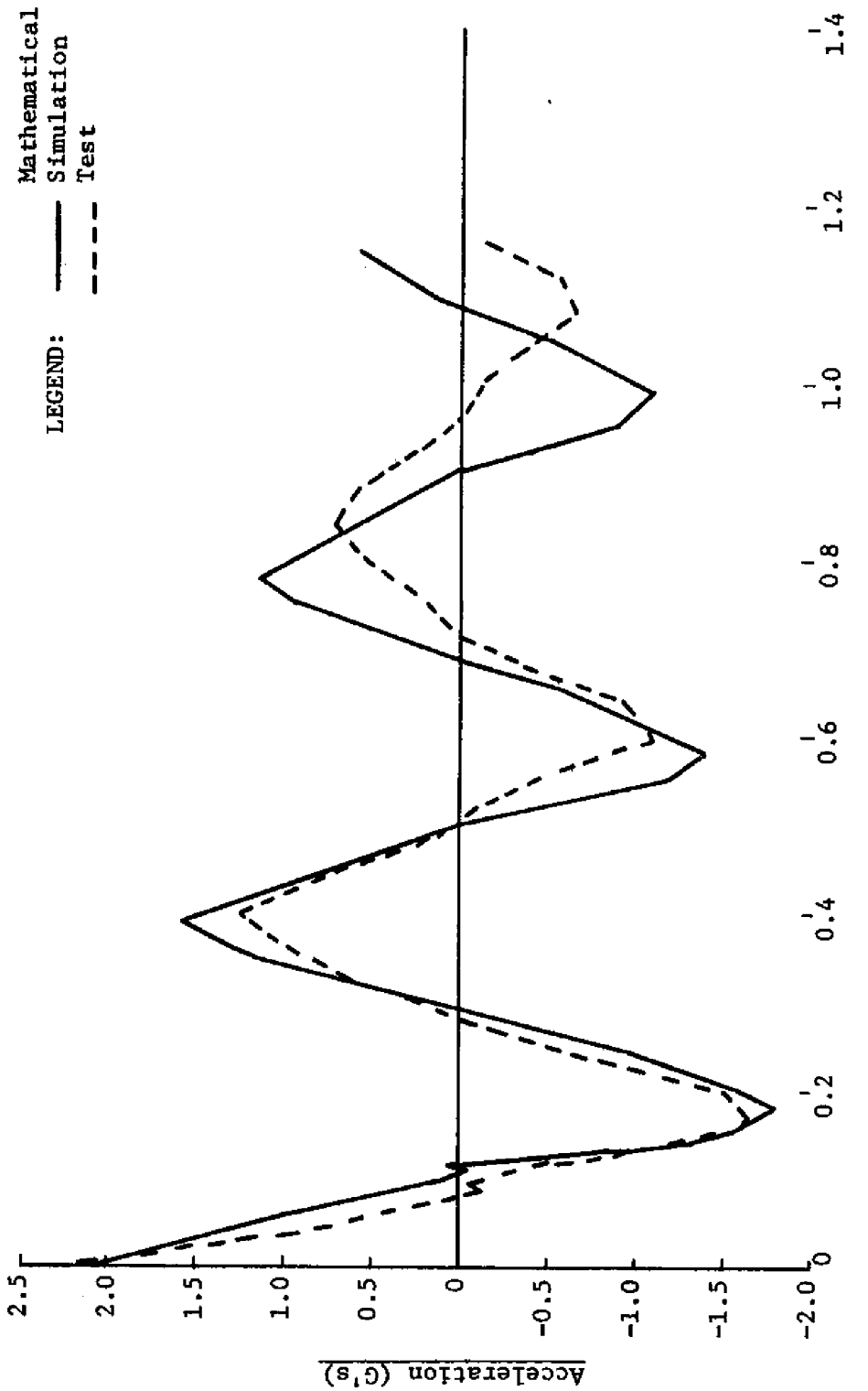

FIGURE 4.9 - ACCELERATION VERSUS TIME, 2.0 INCH PIPE

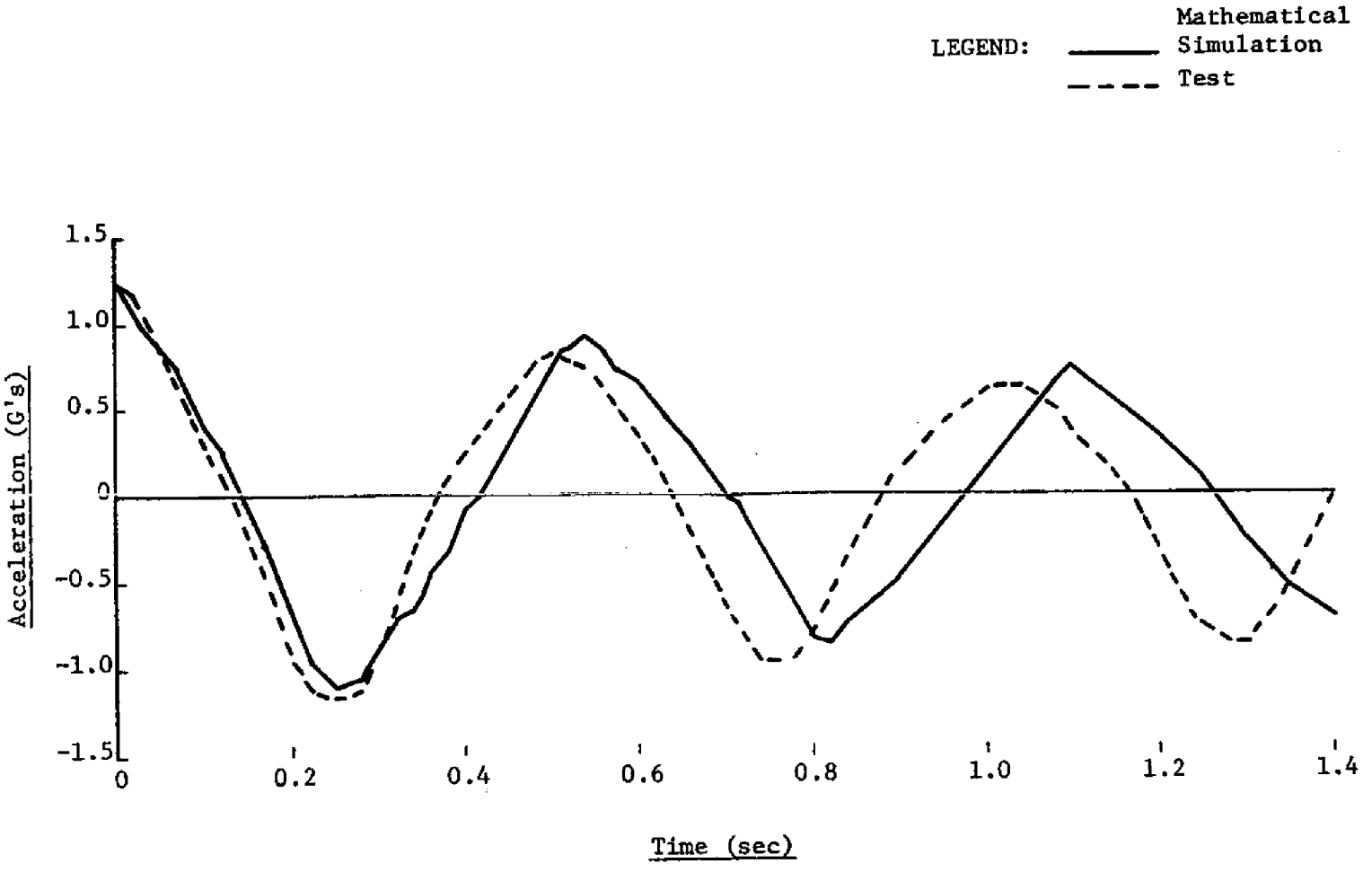

FIGURE 4.10 - ACCELERATION VERSUS TIME, 1.5 INCH PIPE

pipe. During field tests it was noted that the 2.0 inch pipe was not as firmly embedded as the other two pipes. As a result more sliding friction between the pipe wall and adjacent soil likely occurred causing a greater response attenuation. It may be necessary in future analytical model studies to account for sliding friction of this type.

If the 2.0 inch pipe did experience considerable sliding or columb friction, the test results suggest that the amount of soil viscous damping assumed for the mathematical model was excessive. This can be deduced from a consideration of the ratio of structural damping to soil viscous damping. In comparing the simulated response of the three pipe configurations, the percent of critical damping increased with pipe size. As assumed, structural damping offered a constant contribution to the total percent of critical damping, independent of pipe size, and it can therefore be concluded that the increase was a result of increased soil damping. Thus, the error produced by excessive soil damping would be more pronounced at larger pipe sizes.

Although this validation study was limited in scope, the results appear to support the basic approach taken in developing the pipe-soil model. Obviously, more tests are needed, however, of both model and full-scale piles, to further verify the mathematical model's capabilities and to define unknown parameters, such as the damping characteristics of various soils under lateral loads.

A free vibration test was planned for the field studies of the three pipes where the upper part of the pipes would have been surrounded by water. However, difficulties in setting up the tests prevented their successful conclusion. It seems probable, however, that the state-of-the-art in defining the kinetics and kinematics of both the water and wave environment about offshore piles has reached a reliable stage. For this reason, the inability to check the simulated pile's interaction with a water environment is not believed to be a significant obstacle in its validation.

CHAPTER V

PARAMETER STUDIES

5.1 General

In this chapter an effort is made to illustrate the influence of several significant parameters on the pile's response.

The pile utilized in the studies is shown in Figure 5.1. The scale is distorted to clarify the pile's details. To simulate the inertial and stiffness effects of the deck section of an offshore platform, an effective mass of 1,000 in.-lb/sec^2 was added to node 1; and k_H and k_R (reference Figure 2.4) were arbitrarily chosen to be 6,000 lb/in. and 50,000,000 in.-lb/radian, respectively. The large value of k_R was intended to prevent joint rotation at node 1, a situation typical of many offshore platforms. In using this "typical" pile for the parameter studies, the fourth objective of this research was also met, i.e., application of the mathematical solution to obtain the dynamic response of a typical offshore pile.

In all of the studies, the drag coefficient was assumed to equal 1.0 and the coefficient of mass was assumed to equal 1.5. A wave having a 25 foot height, a 10 second period, and a length of 450 feet provided the dynamic loading in each case.

5.2 Distribution of Modulus of Subgrade Reaction

One of the several problems facing designers of pile supported structures is to determine how to distribute the soil's resistance

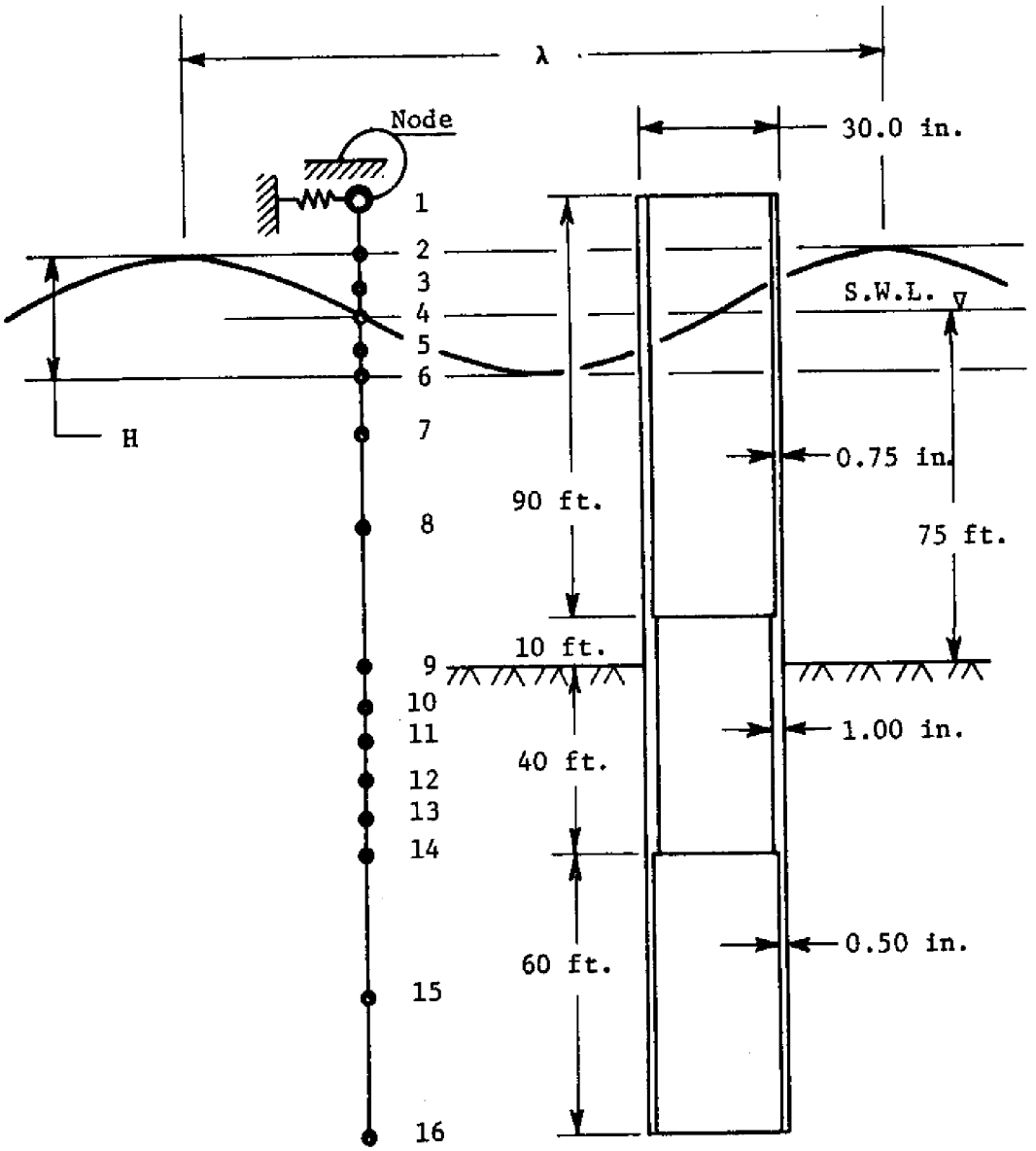

FIGURE 5.1 - TYPICAL PILE AND ITS IDEALIZATION

with depth. To shed some light on the influence such choices have on the response of the pile, four different cases were studied. Details of each case are described in Figure 5.2 and Table 5.1. Note that in case A the pile is assumed to be rigidly fixed 40 feet below the sea bottom.

The initial displacements and velocities of the pile were assumed to be zero. For the soil damping characteristics, J_m was assumed to equal 0.575 sec/in. and L_{mU} was assumed to equal 0.2 in., with both values assumed constant along the embedded length of the pile. It was further assumed that the structural damping factor was 0.079 and that there was no axial load on the pile.

Shown in Figure 5.3 is the lateral displacement of node 6 as a function of time for the four cases. The relative position of the wave with respect to time is shown at the top of the figure, e.g., at 5 seconds the wave trough was located at the pile and at 10 seconds the crest was located there. Node 6 displacements were chosen for illustrative purposes since the lateral displacement of pile reached a maximum at that point.

Displacements based on cases A and B are quite similar. In general, the results were as anticipated, with the displacements decreasing as the degree of fixity increased. The range of maximum displacement was from 1.6 inches for case D to 2.17 inches for case B or a difference of 26 percent.

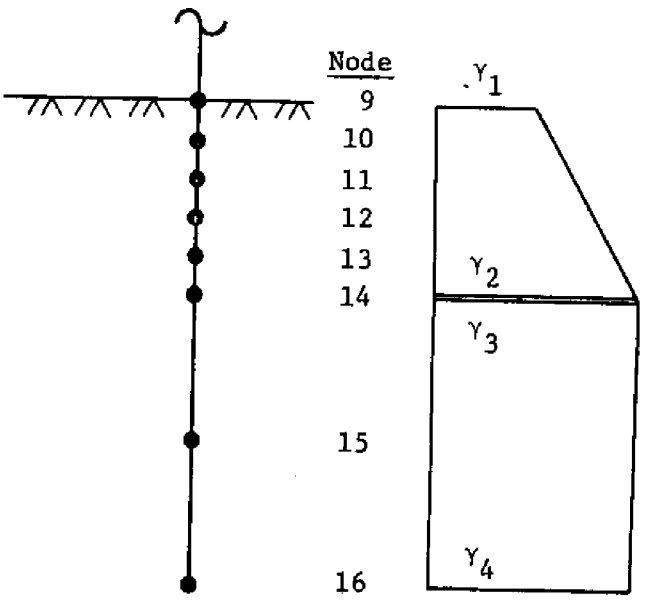

FIGURE 5.2 - SUBGRADE MODULUS DISTRIBUTION

TABLE 5.1 - SUBGRADE DISTRIBUTION DATA

	γ's (lb/in.^{3})			
Case	γ_1	γ_2	γ_3	γ_4
A	0	0	∞	∞
B	0	60	60	150
C	25	150	150	150
D	150	150	150	150

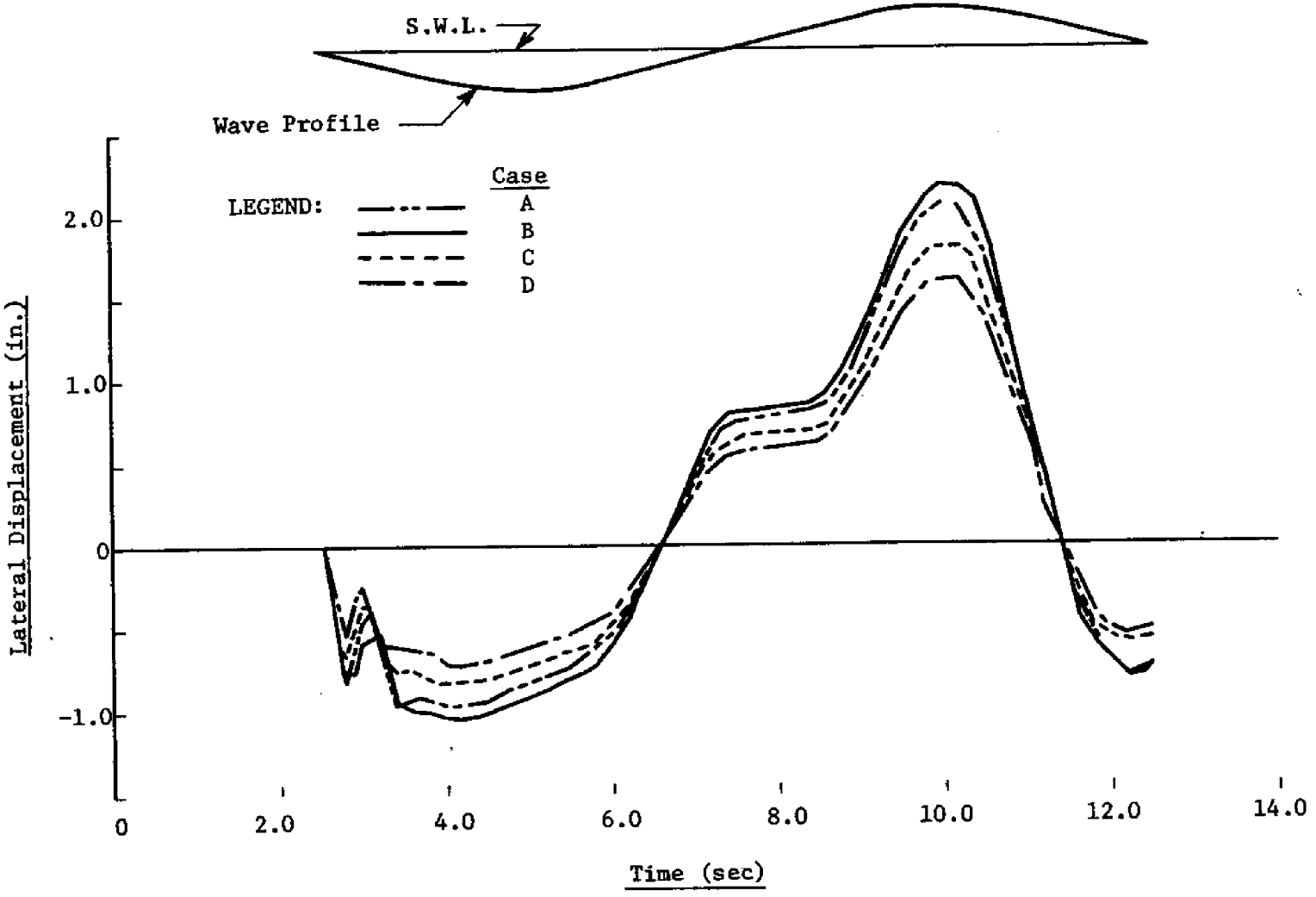

FIGURE 5.3 - NODE 6 DISPLACEMENT VERSUS TIME, SUBGRADE MODULUS STUDY

5.3 Soil Damping

To determine the relative influence of soil damping, case B of the previous section was rerun with J_m equal to zero at all points along the embedded length of the pile. It was further assumed that the stiffness of the soil remained elastic, i.e., L_{mU} was assigned a large value.

Differences in these two conditions was slight, especially along the length of the pile above the mudline. Figure 5.4 shows a plot of lateral displacements at node 9 as a function of time. The differences that do exist occur mainly at changes in the direction of motion.

Although this comparison suggests that soil damping and its nonlinear stiffness characteristics may not be critical, it would be premature to make this conclusion before additional studies are conducted. The stress history of the pile, in particular the portion below the mudline, needs to be investigated rather than just displacements. Future pile studies to be conducted at Texas A&M University should provide valuable data on soil damping.

5.4 Static Versus Dynamic Displacements

Many structures, subject to dynamic loading, are designed by methods of statics, with a factor of safety applied to the loads to account for dynamic effects. The question that always arises is just how large should the factor of safety be. With the

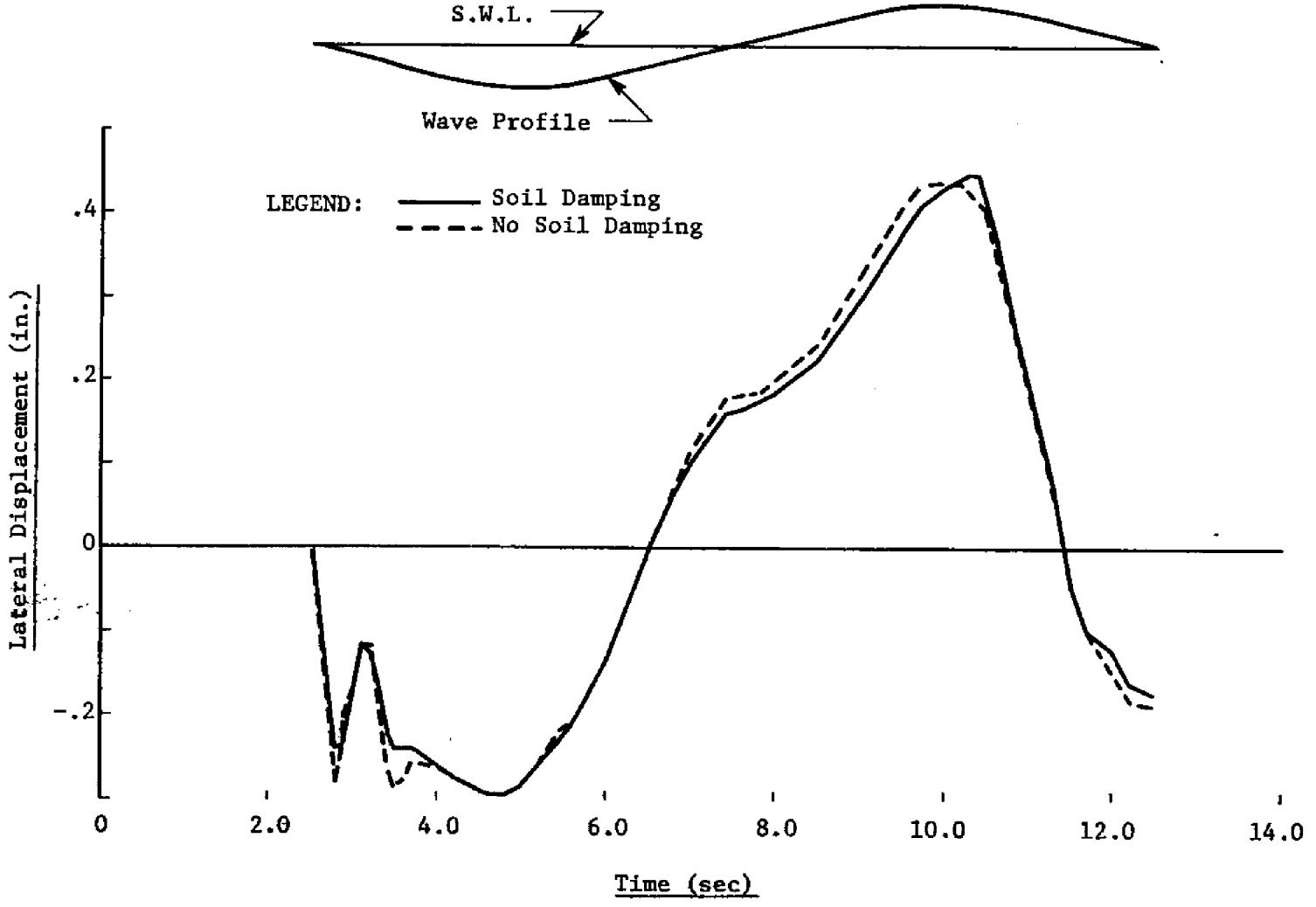

FIGURE 5.4 - NODE 9 DISPLACEMENT VERSUS TIME, SOIL DAMPING STUDY

capabilities of a dynamic model of the type described herein, this uncertainty can be greatly reduced.

Figure 5.5 shows the maximum displaced position of the pile as determined from a static and dynamic analysis of the subject pile. The dynamic conditions were as described in Section 5.2, case B. In the static analysis, the case B static soil properties were used and the loads were those that would exist on a rigid vertical pile when the crest of the wave, described in Section 5.2, passed the pile. The difference is significant along the upper portion of the pile, decreasing considerably along the lower portion.

5.5 Wave-Structure Interaction

In formulating the equations to describe the wave forces (reference equations 2.13 and 2.22), provisions were made to account for the relative velocities and accelerations between the pile and wave particles. This portion of the parameter study was undertaken to determine if such a provision is necessary for the type of problems under consideration. Elimination of the need to consider wave-structure interaction would simplify the analysis and reduce the computer time required for problem solutions.

Figures 5.6 and 5.7 show the lateral displacement of nodes 1 and 6, respectively, versus time, with and without the effects of interaction. These results indicate that wave-structure interaction is an important factor in the dynamic analysis of offshore piling.

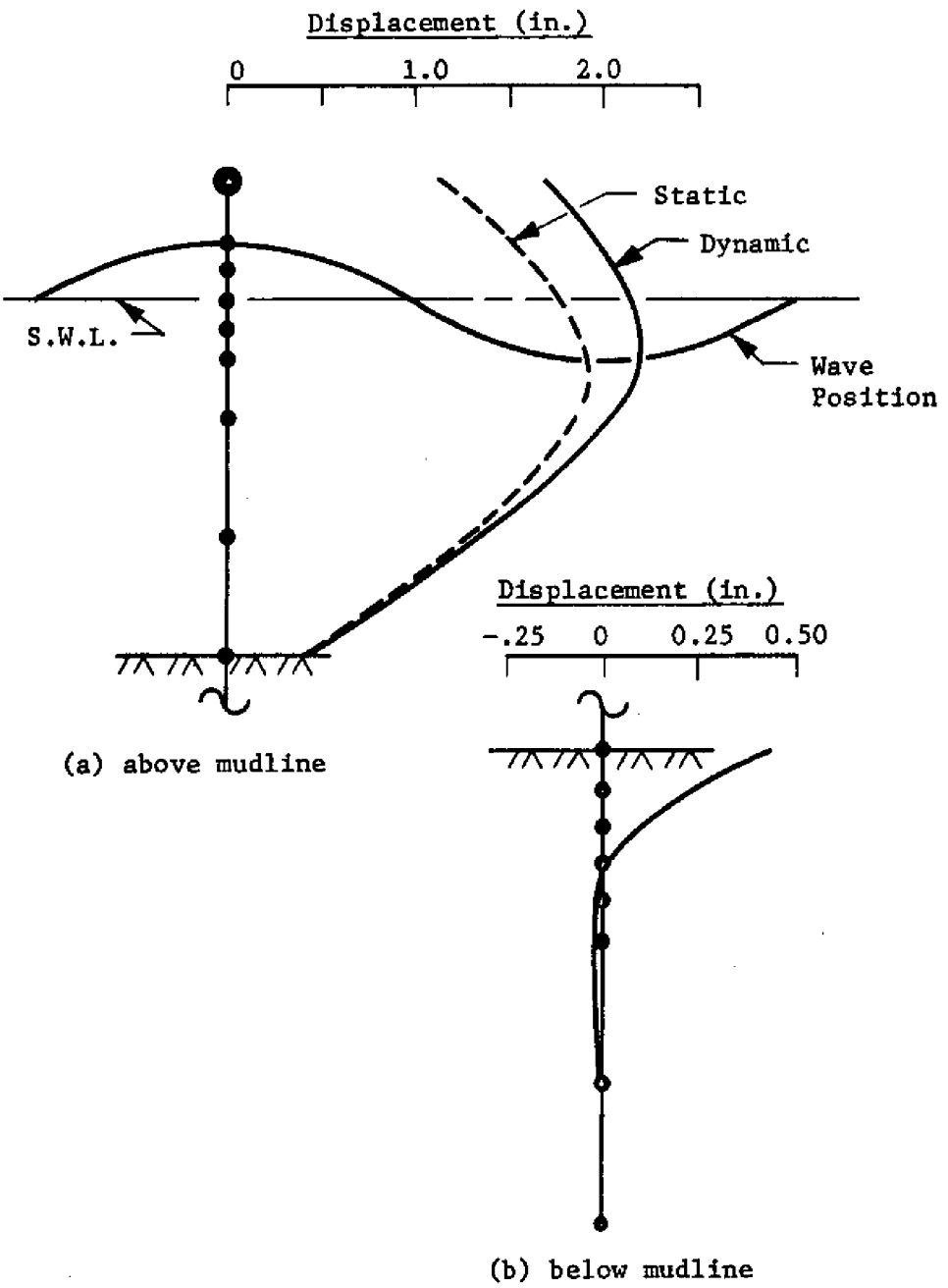

FIGURE 5.5 - MAXIMUM DISPLACEMENTS, CASE B

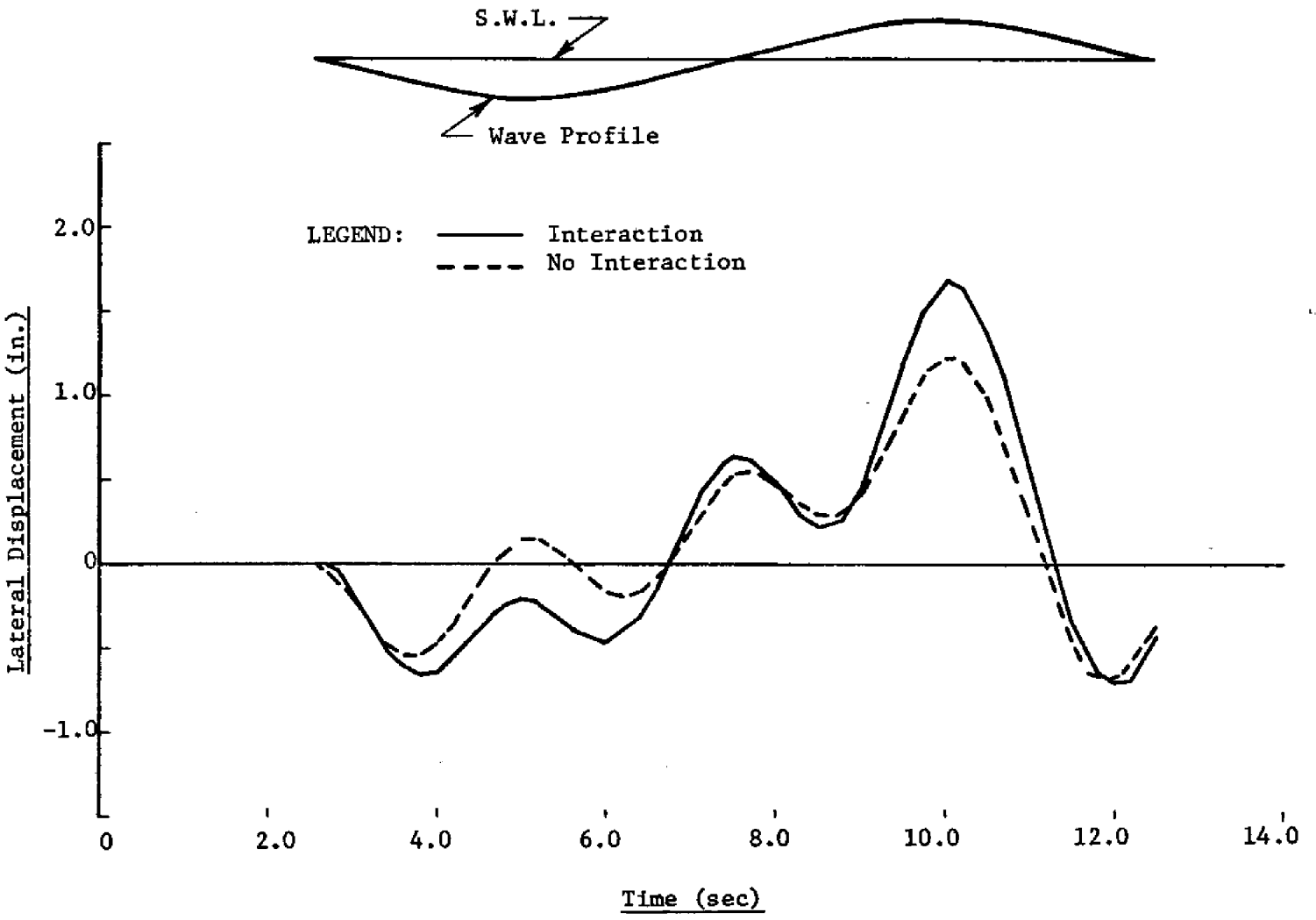

FIGURE 5.6 - NODE 1 DISPLACEMENT VERSUS TIME, INTERACTION STUDY

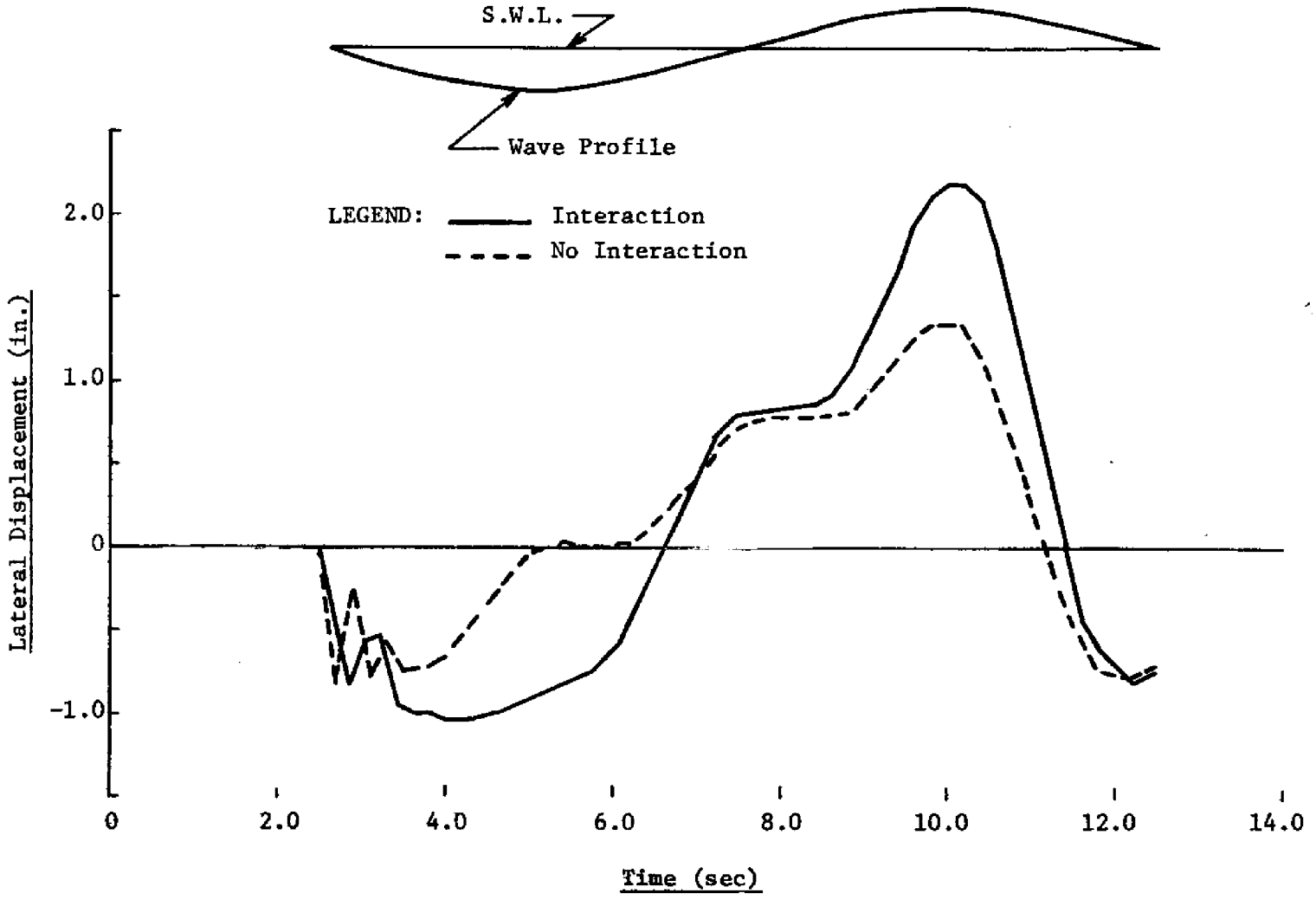

FIGURE 5.7 - NODE 6 DISPLACEMENT VERSUS TIME, INTERACTION STUDY

Maximum displacements in the interaction case are greater than those of the no-interaction case by a factor of approximately 1.6.

It is interesting to note that the frequency of node 1 was approximately 0.4 cycles per second. By a separate analysis (eigenvalue computer program developed by the writer), the fundamental frequency of the pile was computed to be 0.39 cycles per second.

The conditions of this study were identical to that described in Section 5.2. Case B of Table 5.1 was used for the soil resistance.

5.6 Axial Load Effects

Figure 5.8 shows the pile's response for three different axial loads, 400,000 pounds tension, 400,000 pounds compression, and no axial load. The conditions in this study were identical to that described in Section 5.2. Case B of Table 5.1 was used for the soil resistance.

As expected, when compared to the no axial load case, the tensile load reduced the maximum displacement whereas the compressive load acted to increase it. For the upper portion of the pile where the thickness is 0.75 inches, the cross-sectional area is 69.0 square inches and with an axial load of 400,000 pounds the axial stress would be 5,600 pounds per square inch. This stress level is probably typical for offshore piles, and if so, the

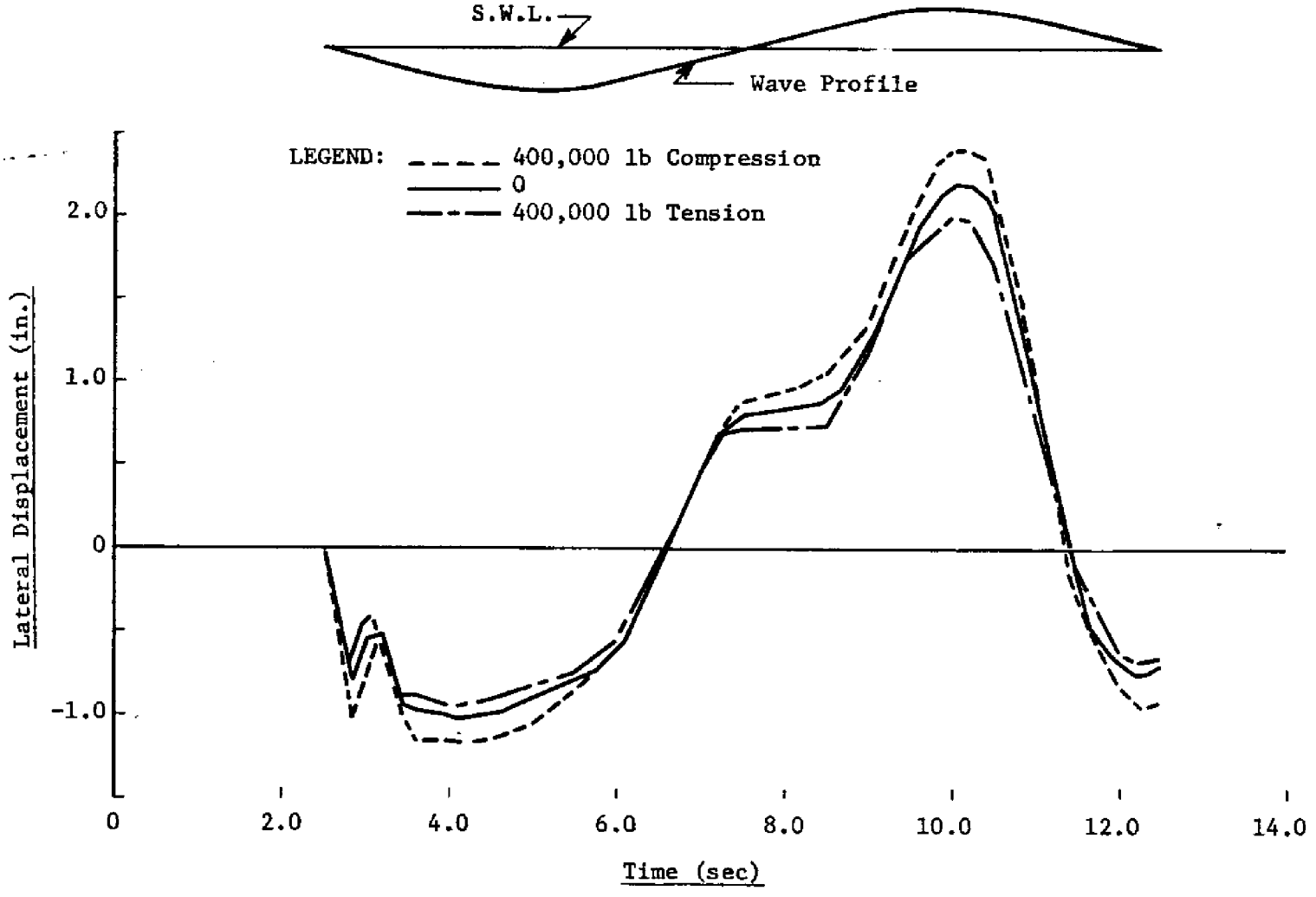

FIGURE 5.8 - NODE 6 DISPLACEMENT VERSUS TIME, AXIAL LOAD STUDY

maximum displacements computed by the no load case may be expected to be in error by as much as ±10 percent, or more.

To account for axial load effects in analyzing the entire offshore platform, the stiffness matrix would have to be modified at each new integration step since the axial load in each member changes accordingly. In the example presented in Figure 5.8, it was assumed that the axial load remained constant throughout the period of analysis.

CHAPTER VI

CONCLUSIONS

The fundamental objective of this research was to develop a mathematical model for determining the dynamic response of an offshore pile subjected to wave loading. The proposed model meets these requirements. It can be applied to study the influence of wave-pile interaction, the effects of a soil medium whose dynamic and static properties are nonlinear, the effects of axial load in the pile, and other factors.

A good comparison was obtained between results from dynamic tests of model piles and simulations of the tests by the mathematical model. Although the experimental tests were necessarily limited, the correlations support the basic approach taken in developing the model.

General conclusions reached as a result of a limited parameter study of a typical offshore pile follow.

1. Magnitude and distribution of the soil subgrade modulus with depth of embedment influences the dynamic response considerably.
2. The soil does not appear to dissipate large amounts of energy of the vibrating system. More studies are needed, however, to verify this observation.

3. Maximum displacements based on dynamic analysis were considerably greater than maximum displacements by static analysis, especially along the upper portion of the pile.
4. Consideration of wave-pile interaction is warranted in the dynamic analysis of offshore piles.
5. Neglecting the axial load effects in the pile may result in an error of ±10 percent in maximum displacements.

In summary, the development of the model described herein should serve to advance the state-of-the-art in design and analysis of offshore pile supported structures. Subject to further comparisons with full-scale tests, the next logical step would be an integration of the proposed model with a model of the complete offshore structure.

CHAPTER VII

RECOMMENDATIONS

The following areas are recommended for further research:

1. To better understand the dynamic properties of soil under lateral loads, additional field tests should be performed. Model piles, similar to those described herein, or possibly full-scale piles, could be instrumented to measure accelerations and stress distributions at selected points along the pile. Tests should be conducted in both cohesive and noncohesive soils.
2. More parameter studies are needed. For example, the effects of prolonged soil failure on the pile's response merits further consideration. In the examples reported, only one complete wave cycle was investigated and the soil was assumed to have no initial soil failure.
3. The computer program should be modified to solve for and print out stress resultants at selected points along the pile. The stress variations with time could then be studied. It is likely that the design of most offshore structures is governed by stresses rather than displacements.
4. The computer program should be modified to permit the consideration of various wave theories. (Airy theory was utilized in this analysis.)

5. Subject to further comparisons with full-scale or model pile tests, the pile model should be integrated with a model of the complete offshore structure.

REFERENCES

1. Agerschon, H. A., and Edens, J. J., "Fifth and First Order Wave-Force Coefficients for Cylindrical Piles," Coastal Engineering, Santa Barbara Specialty Conference, American Society of Civil Engineers, Oct., 1965.

2. Billington, D. P., Gaither, W. S., and Ebner, A. M., "Analysis of Four-Legged Tower for Dynamic Loads," Journal of the Engineering Mechanics Division, Proceedings of the American Society of Civil Engineers, Vol. 92, No. EM2, April, 1966.

3. Chan, P. C., and Hirsch, T. J., "Soil Dynamics and Soil Rheology," Research Report No. 33-5, Texas Transportation Institute, Texas A&M University, June, 1966.

4. Dean, R. G., "Relative Validities of Water Wave Theories," Proceedings of the Conference on Civil Engineering in the Oceans, American Society of Civil Engineers Conference, San Francisco, California, 1967.

5. Dean, R. G., "Stream Function Wave Theory: Validity and Application," Coastal Engineering, Santa Barbara Specialty Conference, American Society of Civil Engineers, Oct., 1965, pp. 269-299.

6. Evans, D. J., "Analysis of Wave Force Data," Preprints of the 1969 Offshore Technology Conference, Houston, Texas, Vol. 1, No. OTC 1005, May, 1969, pp. 51-70.

7. Feibush, R. J., and Keith, E. J., "Analysis of Offshore Structures Including Coupled Structure, Pile and Inelastic Soil Properties," Preprints, First Annual Offshore Technology Conference, Houston, Texas, 1969.

8. Fleming, J. F., Screwvala, F. N., and Konder, R. L., "Foundation Superstructure Interaction Under Earthquake Motion," Proceedings, Third World Conference on Earthquake Engineering, Auckland and Wellington, New Zealand, 1965, pp. I-22 to I-30.

9. Foster, E. T., "Predicting Wave Responses of Deep-Ocean Tower," Proceedings of the Conference on Civil Engineering in the Oceans, American Society of Civil Engineers Conference, San Francisco, Calif., 1967.

10. Gaul, R. D., "Model Study of a Dynamically Laterally Loaded Pile," Journal of the Soil Mechanics and Foundations Division, Proceedings of the American Society of Civil Engineers, Vol. 84, No. SM1, February, 1958.

11. Gibson, G. C., and Coyle, H. M., "Soil Damping Constants Related to Common Soil Properties in Sands and Clays," Research Report No. 125-1, Texas Transportation Institute, Texas A&M University, Sept., 1968.

12. Gill, H. L., "Soil Behavior Around Laterally Loaded Piles," Technical Report R 571, Naval Civil Engineering Laboratory, Port Hueneme, California, April, 1968.

13. Gomez-Rivas, A., "Wave-Structure Interaction in Offshore Platforms," Preprints, First Annual Offshore Technology Conference, Houston, Texas, 1969.

14. Harleman, D. R., Nolan, W. C., and Honsinger, V. C., "Dynamic Analysis of Offshore Piling," Proceedings of the Eighth Conference on Coastal Engineering, Mexico City, Mexico, Nov., 1962, pp. 482-499.

15. Hatano, T., "Vibration of Visco-Elastic Body," Proceedings, Third World Conference on Earthquake Engineering, Auckland and Wellington, New Zealand, 1965, pp. II-126 to II-145.

16. Hayashi, S., and Miyajima, N., "Dynamic Lateral Load Tests on Steel H-Piles," Proceedings, Japan National Symposium on Earthquake Engineering, Tokyo, Japan, 1962.

17. Hayashi, S., Miyajima, N., and Yamashita, I., "Horizontal Resistance of Steel Piles Under Static and Dynamic Loads," Proceedings, Third World Conference on Earthquake Engineering, Auckland and Wellington, New Zealand, 1965, pp. II-146 to II-167.

18. Hurty, W. C., and Rubinstein, M. F., Dynamics of Structures, Prentice-Hall, Inc., Englewood Cliffs, New Jersey, 1964.

19. Iakeda, J., and Tachikawa, H., "Mechanical Properties of Sand Subjected to Dynamic Load by Shallow Footing," Proceedings, Third World Conference on Earthquake Engineering, Auckland and Wellington, New Zealand, 1965, pp. I-180 to I-194.

20. Ippen, A. T. (editor), Estuary and Coastline Hydrodynamics, McGraw-Hill Book Company, Incorporated, 1966, pp. 357-363.

21. Konder, R. L., and Krizek, R. J., "Dynamic Response of Cohesive Soils for Earthquake Considerations," Proceedings, Third World Conference on Earthquake Engineering, Auckland and Wellington, New Zealand, 1965, pp. I-96 to I-106.

22. Lambe, T. W., and Whitman, R. V., Soil Mechanics, John Wiley & Sons, Inc., 1969, page 231.

23. Lowery, L. L., Jr., "Dynamic Behavior of Piling," A dissertation submitted to the Graduate College, Texas A&M University, in partial fulfillment of the requirements for the degree of Doctor of Philosophy, May, 1967.

24. McCormick, J. M., and Salvadori, M. G., Numerical Methods in Fortran, Prentice-Hall, Inc., 1965, p. 103.

25. Matlock, H., and Reese, L. C., "Generalized Solutions for Laterally Loaded Piles," Proceedings, American Society of Civil Engineers, Vol. 86, No. SM5, Oct., 1960.

26. Matsumoto, Y., and Tsuchiya, T., "Lateral Load Capacity of Vertical and Battered Concrete Pile Groups," Proceedings, Japan National Symposium on Earthquake Engineering, Tokyo, Japan, 1962.

27. Michalos, J., "Dynamic Response and Stability of Piers on Piles," Journal of the Waterways and Harbors Division, American Society of Civil Engineers, Vol. 88, No. WW3, Aug., 1962.

28. Mindlin, R. D., "Force at a Point in the Interior of a Semi-Infinite Solid," Physics, Vol. 7, May, 1956.

29. Morison, J. R., O'Brien, M. P., Johnson, J. W., and Schaaf, S. A., "The Force Exerted by Surface Waves on Piles," Journal of Petroleum Technology, American Institute of Mining and Metallurgical Engineers, Vol. 2, No. 5, 1950.

30. Nath, J. H., and Harleman, D. R. F., "The Dynamics of Fixed Towers in Deep Water Random Waves," Proceedings of the Conference on Civil Engineering in the Oceans, American Society of Civil Engineers Conference, San Francisco, Calif., 1967.

31. Penzien, J., et al, "Seismic Analysis of Bridges on Long Piles," Journal of the Engineering Mechanics Division, Proceedings of the American Society of Civil Engineers, Vol. 90, No. EM3, June, 1964.

32. Prakash, S., and Aggarwal, S. L., "Study of a Vertical Pile Under Dynamic Lateral Load," Proceedings, Third World Conference on Earthquake Engineering, Auckland and Wellington, New Zealand, 1965, pp. I-215 to I-229.

33. Przemieniecki, J. S., Theory of Matrix Structural Analysis, McGraw-Hill Publishing Company, New York, 1968.

34. Reese, L. C., and Haliburton, T. A., Discussion of "Dynamic Response and Stability of Piers on Piles," Journal of Waterways and Harbors Division, American Society of Civil Engineers, No. WW2: May 63: 85: 3527.

35. Rehmet, J. D., and Coyle, H. M., "Preliminary Study of In-Situ Measurements of Friction and Bearing in Clay," Research Report 125-3, Texas Transportation Institute, Texas A&M University, Sept., 1969.

36. Samson, C. H., Jr., Hirsch, T. J., and Lowery, L. L., Jr., "Computer Study of Dynamic Behavior of Piling," Journal of the Structural Division, American Society of Civil Engineers, Paper No. 3608, ST4, Aug., 1963.

37. Shubinski, R. P., Wilson, E. L., and Selna, L. G., "Dynamic Response of Deepwater Structures," Proceedings of the Conference on Civil Engineering in the Oceans, American Society of Civil Engineers Conference, San Francisco, California, 1967.

38. Smith, E. A. L., "Pile-Driving Analysis by the Wave Equation," Journal of the Soil Mechanics and Foundations Division, American Society of Civil Engineers, Paper No. 2574, SM4, Aug., 1960.

39. Spillers, W. R., and Stoll, R. D., "Lateral Response of Piles," Journal of the Soil Mechanics and Foundations Division, Proceedings of the American Society of Civil Engineers, Vol. 90, No. SM6, Nov., 1964.

40. Taylor, P. W., and Hughes, J. M. O., "Dynamic Properties of Foundation Subsoils as Determined From Laboratory Tests," Proceedings, Third World Conference on Earthquake Engineering, Auckland and Wellington, New Zealand, 1965, p. I-196 to I-212.

41. Timoshenko, S., Vibration Problems in Engineering, D. Van Nostrand Co., Inc., Princeton, New Jersey, 1955, p. 377.

42. Wilson, B. W., and Reid, R. O., Discussion of Wave-Force Coefficients for Offshore Pipelines," Journal of Waterways and Harbors Division, Proceedings of American Society of Civil Engineers, Feb., 1963, pp. 61-65.

43. Zienkiewicz, O. C., The Finite Element Method in Structural and Continuum Mechanics, McGraw-Hill Publishing Company, London, 1967.

APPENDIX I

COMPUTER PROGRAM DESCRIPTION

COMPUTER PROGRAM DESCRIPTION

A simplified flow chart of the program used in the analysis is shown in Figure A1. Items up to point B in the chart are completed in the calling or MAIN program. At point B the program branches and one of six possible paths is taken. Each of the six cases is a subprogram containing fourth-order Runge-Kutta solutions for six distinct situations. The characteristics of each case are described in Table A1. By using the six cases a more efficient program was possible.

Examples described in Chapter V were run on an IBM 360/65 computer. Each example required approximately six minutes of computer time.

Output from the program consists of displacements, velocities, and accelerations at each node. Also printed out at the termination of each run are the values of both positive and negative permanent set which occurs during the event.

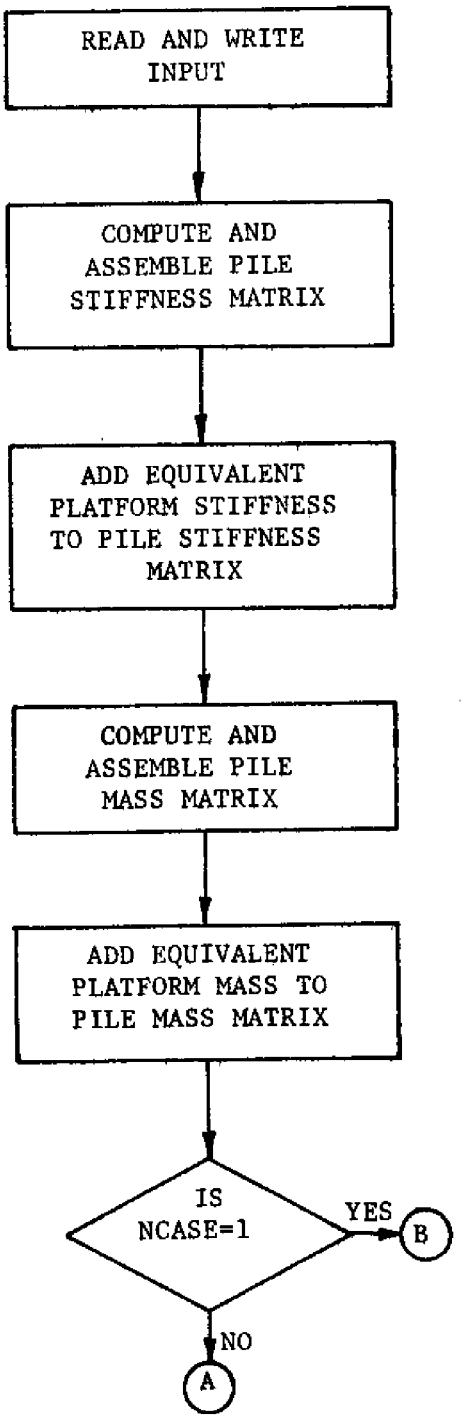

FIGURE A1 - FLOW CHART

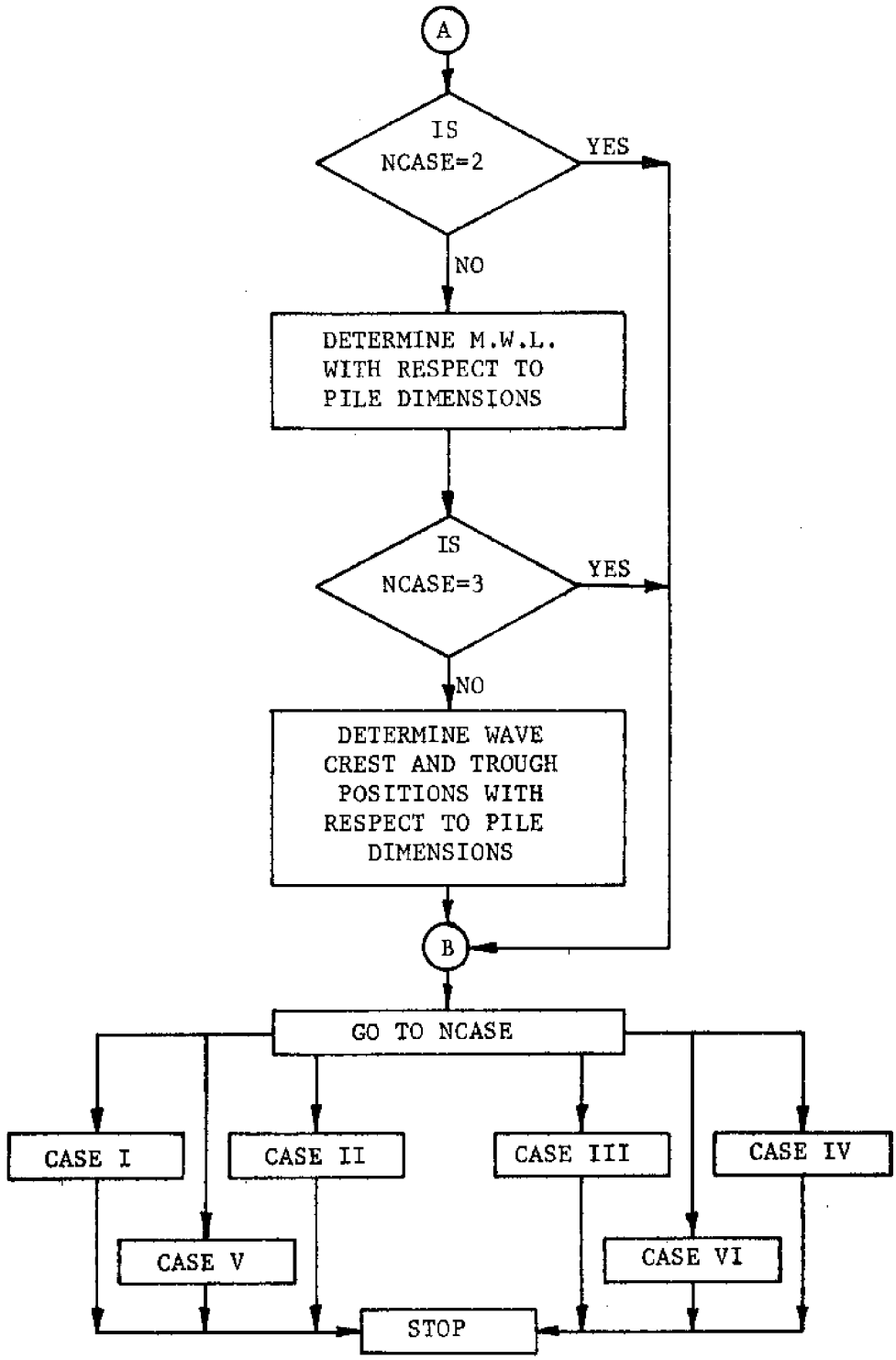

FIGURE A1 - (CON'T)

TABLE A1 - RUNGE-KUTTA CASE CHARACTERISTICS

	Soil Static Properties		Type of Damping		Type of Vibration		Water Environment[b]	Wave - Structure Interaction?	
Case	Linear	Non-Linear	Soil	Structural	Free	Forced[a]		Yes	No
I	X				X				
II		X			X				
III		X	X	X	X				
IV		X	X	X	X		X		
V		X	X	X		X	X	X	
VI		X	X	X		X	X		X

[a] By wave computed according to linear theory.
[b] Water surrounds the pile from the sea bottom to some height above the bottom.

APPENDIX II

COMPUTER PROGRAM INPUT

COMPUTER PROGRAM INPUT

Input Definitions

The following symbols are used in the program input:

BCDISP(J,1) = an array containing the initial node displacements, in.;

BCVEL(J,1) = an array containing the initial node velocities, in./sec;

DATE(J) = an array containing the date of the test or computer run;

DELTAT = numerical integration increment, sec;

ELPROP(J,K) = an array containing pile segment properties;
for pile segment J,
ELPROP(J,1) = diameter of segment, in.;
ELPROP(J,2) = length of segment, in.;
ELPROP(J,3) = cross-sectional area of segment, $in.^2$;
ELPROP(J,4) = second moment of area of segment, $in.^4$;
ELPROP(J,5) = modulus of elasticity of segment, $lb/in.^2$;
ELPROP(J,6) = weight density of segment material, $lb/in.^3$;

ELSOIL(J,K) = an array containing the soil element properties;
for element J,
ELSOIL(J,1) = soil stiffness, lb/in.;
ELSOIL(J,2) = soil damping factor (J_m), sec/in.;
ELSOIL(J,3) = soil damping factor (n_m), dimensionless;

ELSOIL(J,4) = soil density, lb/in.^{3};

ELSOIL(J,5) = ultimate displacement of soil (L_{mu}), in.;

ESSAG(J) = an array containing identification of the test or computer run;

NCASE = Runge-Kutta case (See Table A1);

NITER = number of time increments (DELTAT) to be computed (NITER multiplied by DELTAT equals the real time of the event);

NOP1 = option code; if NOP1 = 0, individual pile segment properties must be input, and if NOP1 = 1, all pile segments possess the same properties;

NOS1 = option code; if NOS1 = 0, individual soil element properties must be input, and if NOS1 = 1, all soil elements possess the same properties;

NOW1 = option code; if NOW1 = 0, nodal velocities are not printed out, and if NOW2 = 1, nodal velocities are printed out;

NOW2 = option code; if NOW2 = 0, nodal accelerations are not printed out, and if NOW2 = 1, nodal accelerations are printed out;

NUMM = total number of pile segments;

NUMMTP = number of pile segments above midline;

NWRITE = output print interval;

PAREA = cross-sectional area of pile, in.^{2};

PDEN = weight density of pile material, lb/in.^{3};

PDIA = pile diameter, in.;

PELAS = modulus of elasticity of pile, lb/in.^{2};

PKTOPH = equivalent lateral platform stiffness (k_H), lb/in.;

PKTOPR = equivalent rotational platform stiffness (k_R), in.-lb/rad;

PLEN = length of pile segments, in.;

PLOAD = axial load in pile (+ if tension and - if compression), lb;

PMTOP = equivalent platform mass, lb-sec^2/in.;

PINERT = second moment of area of pile, in.^{4};

PSETP(J) = an array containing initial values of the permanent set in the positive direction (PPS_m) of each soil element, in.;

PSETN(J) = an array containing initial values of the permanent set in the hegative direction (PNS_m) of each soil element, in.;

SDMCOE = structural damping factor (μ), dimensionless;

SOILC = soil damping factor (J_m), sec/in.;

SOILD = soil density, lb/in.^{3};

SOILK = stiffness of soil elements, lb/in.;

SOILMC = soil mass coefficient, dimensionless;

SOILN = soil damping factor (n_m), dimensionless;

SOILUL = ultimate displacement of soil (L_{mu}), in.;

TEMPP(J) = an array containing initial maximum nodal displacements from the mudline to the bottom of the pile in the

positive direction, in.;

TEMPN(J) = an array containing initial maximum nodal displacements from the mudline to the bottom of the pile in the negative direction, in.;

TIMEI = time at which solution is to be initiated, sec;

UPPLIM = maximum value of lateral displacement of node 1 permitted (if exceeded the program is terminated), in.;

VELOO = nodal velocity at which the structural damping is completely effective, in./sec;

WAVEH = wave height, in.;

WAVEL = wave length, in.;

WAVET = wave period, sec;

WDEN = water density, $lb/in.^3$;

WDRAG = drag coefficient, dimensionless;

WMASS = mass coefficient, dimensionless; and

YWAT = depth of water, in.

Input Format

I. First card

Item	Column	Format
ESSAG	1-80	A

II. Second card

Item	Column	Format
DATE	1-20	A

III. Third card

Item	Column	Format
NUMM	1-5	I (right justified)
NUMMTP	6-10	I (right justified)
NCASE	11-15	I (right justified)
NOW1	16-20	I (right justified)
NOW2	21-25	I (right justified)
NOP1	26-30	I (right justified)
NOS1	31-35	I (right justified)

IV. Fourth card (omit if NOP1 = 0)

Item	Column	Format
PDIA	1-10	F (punch decimal)
PLEN	11-20	F (punch decimal)
PAREA	21-30	F (punch decimal)
PINERT	31-40	F (punch decimal)
PELAS	41-50	F (punch decimal)
PDEN	51-60	F (punch decimal)

V. Next series of cards (omit if NOP1 = 1)

Pile segment properties are input in sequential order beginning with segment 1. There are as many cards in this series as there are pile segments. For segment J the input is as follows:

Item	Column	Format
ELPROP(J,1)	1-10	F (punch decimal)
ELPROP(J,2)	11-20	F (punch decimal)
ELPROP(J,3)	21-30	F (punch decimal)
ELPROP(J,4)	31-40	F (punch decimal)
ELPROP(J,5)	41-50	F (punch decimal)
ELPROP(J,6)	51-60	F (punch decimal)

VI. Next card (omit if NOS1 = 0)

Item	Column	Format
SOILK	1-10	F (punch decimal)
SOILC	11-20	F (punch decimal)
SOILN	21-30	F (punch decimal)
SOILD[a]	31-40	F (punch decimal)
SOILUL	41-50	F (punch decimal)

[a]It is suggested that this be set equal to zero.

VII. Next series of cards (omit if NOS1 = 1)

Soil element properties are input in sequential order beginning with the element at the mudline. There are as many cards in this series as there are soil elements. For element J the input is as follows:

Item	Column	Format
ELSOIL(J,1)	1-10	F (punch decimal)
ELSOIL(J,2)	11-20	F (punch decimal)
ELSOIL(J,3)	21-30	F (punch decimal)
ELSOIL(J,4)[a]	31-40	F (punch decimal)
ELSOIL(J,5)	41-50	F (punch decimal)

[a]It is suggested that this be set equal to zero.

VIII. Next card

Item	Column	Format
PKTOPH	1-20	F (punch decimal)
PKTOPR	21-40	F (punch decimal)
PLOAD	41-50	F (punch decimal)
PMTOP	51-60	F (punch decimal)
SOILMC[a]	61-70	F (punch decimal)

[a]It is suggested that this be set equal to zero.

IX. Next card

Item	Column	Format
SDMCOE	1-10	F (punch decimal)
VELOO[a]	11-20	F (punch decimal)

[a]It is suggested that this be set equal to 0.1.

X. Next card

Item	Column	Format
DELTAT	1-10	F (punch decimal)
TIMEI	11-20	F (punch decimal)
UPPLIM	21-30	F (punch decimal)

Item	Column	Format
NWRITE	31-35	I (right justified)
NITER	36-40	I (right justified)

XI. Next series of cards

This series of cards contain the initial displacements of each node. Initial displacements are input in sequential order beginning with node 1. Eight values are allowed per card. The first card of the series is as follows (assuming there are at least 8 nodes):

Item	Column	Format
BCDISP(1,1)	1-10	F (punch decimal)
BCDISP(2,1)	11-20	F (punch decimal)
BCDISP(3,1)	21-30	F (punch decimal)
BCDISP(4,1)	31-40	F (punch decimal)
BCDISP(5,1)	41-50	F (punch decimal)
BCDISP(6,1)	51-60	F (punch decimal)
BCDISP(7,1)	61-70	F (punch decimal)
BCDISP(8,1)	71-80	F (punch decimal)

If needed, the next card contains BCDISP(9,1) through BCDISP(16,1), etc.

XII. Next series of cards

This series of cards contain the initial velocities of each node. Initial velocities are input in sequential order beginning with node 1. Eight values are allowed per card. The first card of the series is as follows (assuming there are

at least 8 nodes):

Item	Column	Format
BCVEL(1,1)	1-10	F (punch decimal)
BCVEL(2,1)	11-20	F (punch decimal)
BCVEL(3,1)	21-30	F (punch decimal)
BCVEL(4,1)	31-40	F (punch decimal)
BCVEL(5,1)	41-50	F (punch decimal)
BCVEL(6,1)	51-60	F (punch decimal)
BCVEL(7,1)	61-70	F (punch decimal)
BCVEL(8,1)	71-80	F (punch decimal)

If needed the next card contains BCVEL(9,1) through BCDVEL(16,1), etc.

NOTE: No further input required if NCASE = 1.

XIII. Next series of cards

This series contains the initial values of the soil permanent set in the positive displacement direction. Values are input in sequential order beginning with the node at the mudline. The first card of the series is as follows (assuming there are at least 8 nodes from the mudline to the bottom of the pile):

Item	Column	Format
PSETP(1)	1-10	F (punch decimal)
PSETP(2)	11-20	F (punch decimal)
PSETP(3)	21-30	F (punch decimal)
PSETP(4)	31-40	F (punch decimal)

Item	Column	Format
PSETP(5)	41-50	F (punch decimal)
PSETP(6)	51-60	F (punch decimal)
PSETP(7)	61-70	F (punch decimal)
PSETP(8)	71-80	F (punch decimal)

If needed, the next card contains PSETP(9) through PSETP(16), etc.

XIV. Next series of cards

This series contains the initial values of the soil permanent set in the negative displacement direction. Values are input in sequential order beginning with the node at the mudline. The first card of the series is as follows (assuming there are at least 8 nodes from the mudline to the bottom of the pile):

Item	Column	Format
PSETN(1)	1-10	F (punch decimal)
PSETN(2)	11-20	F (punch decimal)
PSETN(3)	21-30	F (punch decimal)
PSETN(4)	31-40	F (punch decimal)
PSETN(5)	41-50	F (punch decimal)
PSETN(6)	51-60	F (punch decimal)
PSETN(7)	61-70	F (punch decimal)
PSETN(8)	71-80	F (punch decimal)

If needed, the next card contains PSETN(9) through PSETN(16), etc.

XV. Next series of cards

This series contains the initial values of the maximum nodal displacements in the positive direction from the mudline to the bottom of the pile. Values are input in sequential order beginning with the node at the mudline. The first card of the series is as follows (assuming there are at least 8 nodes from the mudline to the bottom of the pile):

Item	Column	Format
TEMPP(1)	1-10	F (punch decimal)
TEMPP(2)	11-20	F (punch decimal)
TEMPP(3)	21-30	F (punch decimal)
TEMPP(4)	31-40	F (punch decimal)
TEMPP(5)	41-50	F (punch decimal)
TEMPP(6)	51-60	F (punch decimal)
TEMPP(7)	61-70	F (punch decimal)
TEMPP(8)	71-80	F (punch decimal)

If needed, the next card contains TEMPP(9) through TEMPP(16), etc.

XVI. Next series of cards

This series contains the initial values of the maximum nodal displacements in the negative direction from the mudline to the bottom of the pile. Values are input in sequential order beginning with the node at the mudline. The first card of the series is as follows (assuming there are at least 8 nodes from the mudline to the bottom of the pile):

Item	Column	Format
TEMPN(1)	1-10	F (punch decimal)
TEMPN(2)	11-20	F (punch decimal)
TEMPN(3)	21-30	F (punch decimal)
TEMPN(4)	31-40	F (punch decimal)
TEMPN(5)	41-50	F (punch decimal)
TEMPN(6)	51-60	F (punch decimal)
TEMPN(7)	61-70	F (punch decimal)
TEMPN(8)	71-80	F (punch decimal)

If needed, the next card contains TEMPN(9) through TEMPN(16), etc.

NOTE: No further input required if NCASE $\leq$ 3.

XVII. Next card

Item	Column	Format
YWAT	1-10	F (punch decimal)
WDEN	11-20	F (punch decimal)
WDRAG	21-30	F (punch decimal)
WMASS	31-40	F (punch decimal)

NOTE: No further input required if NCASE $\leq$ 4.

XVIII. Next card (final card)

Item	Column	Format
WAVET	1-10	F (punch decimal)
WAVEL	11-20	F (punch decimal)
WAVEH	21-30	F (punch decimal)

NOTE: Additional problems can be run by repeating the appropriate input in items I through XVIII.

APPENDIX III

NOTATION

NOTATION

The following symbols are used in this paper:

A = cross-sectional area;

$a(z,t)$ = water particle acceleration at depth z and time t;

C_D = drag coefficient;

C_I = inertia coefficient;

D_z = diameter of pile at depth z;

E = modulus of elasticity;

F = axial load in any pile segment, see Equation 2.6;

$F_i(t)$ = concentrated wave force at node i at time t;

$\{F(t)\}$ = matrix of concentrated wave forces;

$f(z,t)$ = wave force in horizontal direction per unit length at depth z and time t;

g = gravitational acceleration;

H = wave height;

h = water depth;

I = area moment of inertia;

J_m = soil viscous damping constant;

$[k] = [k_e] + [k_g]$;

$[k_e]$ = matrix of linearly elastic stiffness coefficients of any pile segment;

$[k_g]$ = matrix of "geometrical" stiffness coefficients of any pile segment;

k_H = lateral stiffness of platform;

$K_{iD} = \frac{1}{2} C_D \rho D_i$;

$K_{iI} = C_I \rho \frac{\pi D_i^2}{4}$;

K_{ms} = lateral stiffness of soil at node m;

$[K^p]$ = matrix of stiffness coefficients of assembled pile segments;

k_R = rotational stiffness of platform;

$[K_R^p]$ = matrix of reduced stiffness coefficients of pile;

L_i = length of pile segment i;

L_{mU} = lateral deformation of soil at node m at which P_{mU} is reached;

[M] = diagonal matrix containing lumped masses;

M_i = lumped mass at node i;

$\{N_1\}$, $\{N_2\}$, $\{N_3\}$, $\{N_4\}$ = matrix of multipliers used in computing the spring and damping forces of the soil;

n_m = soil viscous damping constant;

{P} = matrix of total soil forces acting on pile;

$\{P_d\}$ = matrix of soil damping forces;

$P_m = P_{md} + P_{ms}$

P_{md} = soil damping force at node m;

P_{ms} = soil static resistance in soil spring at node m;

P_{mU} = failure or ultimate lateral load of soil at node m;

PNS_m = amount of negative permanent set of soil at node m;

PPS_m = amount of positive permanent set of soil at node m;

$\{P_s\}$ = matrix of soil static resistance in soil springs;

$\{Q\}$ = matrix of node displacements;

$\{q\}$ = matrix of generalized end displacements of any pile segment;

q_i = generalized displacement at end of any pile segment, i = 1,2,...,6;

$Q_{i,j}$, $\dot{Q}_{i,j}$, $\ddot{Q}_{i,j}$ = displacement, velocity, and acceleration, respectively, at node i in j direction;

$r_i = h + z_i$;

R_n = Reynolds number;

$\{S\}$ = matrix of external loads;

$\{s\}$ = matrix of stress resultants at end of any pile segment;

$\{S_D\}$ = matrix of structural damping forces;

$\{S_{DL}\}$ = matrix of structural damping forces associated with lateral degrees of freedom;

s_i = stress resultant at end of any pile segment, i = 1,2,...,6;

$S_{i,j}$ = external load at node i in j direction;

t = time;

$v(z,t)$ = water particle velocity at depth z and time t;

w_i = weight of segment i per unit length;

x = horizontal coordinate;

z_i = distance from still water level to node i;

μ = structural damping factor;

σ = wave angular frequency;

β = wave number;

λ = wave length;

η = instantaneous vertical displacement of water surface profile above or below still water level;

Δt = time increment of integration;

δ = pile model deformation;

γ_s = soil modulus of subgrade reaction;

$[\ ]$ = square matrix;

$\{\ \}$ = column matrix;

$\lfloor\ \rfloor$ = transpose of column matrix; and

$|\ |$ = absolute value.